

Binary black hole initial data from matched asymptotic expansions

Nicolás Yunes,¹ Wolfgang Tichy,^{1,2} Benjamin J. Owen,¹ and Bernd Brügmann^{1,3}

¹*Institute for Gravitational Physics and Geometry,
Center for Gravitational Wave Physics, Department of Physics,
The Pennsylvania State University, University Park, PA 16802-6300*

²*Department of Physics, Florida Atlantic University, Boca Raton, FL 33431*

³*Physikalisch-Astronomische Fakultät, Friedrich-Schiller-Universität Jena, 07743 Jena, Germany*

(Dated: Id: paper.tex,v 1.128 2005/03/01 22:12:35 yunes Exp)

We present an astrophysically realistic approximate metric for a binary black hole spacetime to construct initial data for numerical relativity. This metric is obtained by asymptotically matching a post-Newtonian metric for a binary system to a perturbed Schwarzschild metric for each hole. In the *inner zone* near each hole, the metric is given by the Schwarzschild solution plus a quadrupolar perturbation corresponding to an external tidal gravitational field. In the *near zone*, well outside each black hole but less than a reduced wavelength from the center of mass of the binary, the metric is given by a post-Newtonian expansion including the lowest-order deviations from flat spacetime. When the near zone overlaps each inner zone in a *buffer zone*, the post-Newtonian and perturbed Schwarzschild metrics can be asymptotically matched to each other. By demanding matching (over a 3-volume in the buffer zone) rather than patching (choosing a particular 2-surface in the buffer zone), we guarantee that the errors are everywhere small in a well-defined sense. The resulting piecewise metric is made formally globally C^∞ with smooth transition functions so as to obtain the finite extrinsic curvature of a 3-slice as initial data for numerical relativity. In addition to the metric, we present explicit results for the extrinsic curvature, lapse, and shift, which can be used as initial data for numerical simulations. Our approximation gives good results for black holes of arbitrary mass ratio separated by as little as seven times the total mass. This paper lays the foundations of a method that can be straightforwardly iterated to obtain initial data to higher perturbative order.

PACS numbers: 04.25.Dm, 04.25.Nx, 04.30.Db, 95.30.Sf

I. INTRODUCTION

The simulation of binary black-hole systems is of fundamental physical interest as the purely general relativistic two-body problem. It is also of astrophysical interest, since accurate simulations of the late inspiral and merger phases of such binaries will considerably help the effort to detect the gravitational-wave signals and extract information from them [1]. Simulation reduces to the numerical solution of the Cauchy problem: Take some initial data and evolve it. The evolution is difficult for many reasons, although in recent years there has been much progress. Still, any evolution is only as good as its initial data.

The key problem with initial data is astrophysical realism. By now the literature provides many types of initial data for black holes in approximately circular orbits [2, 3, 4, 5, 6, 7, 8, 9, 10, 11, 12, 13, 14] that satisfy the constraints of the Einstein equations, but all suffer various problems. Most approaches to initial data in the literature use a conformal decomposition, in which an auxiliary metric is constructed based on some assumption and then a conformal factor is found that forces the entire metric to obey the constraints. The assumptions are sometimes problematic—for example, conformal flatness is often assumed for convenience, but is known to be violated by the astrophysical spacetime at 2nd post-Newtonian (2PN) order [15]. More generally, any auxiliary metric which is constructed based on some physical intuition will change its properties once it is forced to

obey the constraint equations [8]. Hence, any physical parameters (mass ratio, etc.) that were present in the auxiliary metric will be distorted in the constraint preserving metric.

An astrophysically relevant approximate spacetime can be obtained far from the black holes by analytical post-Newtonian and post-Minkowski methods [15]. While formally these methods assume slow motion and weak internal gravity of the sources, it has been shown that the results hold as well for objects such as black holes with strong internal gravity [16]. Near each black hole, a tidally perturbed Schwarzschild or Kerr spacetime provides another analytical approximation. Given that different approximate metrics can be constructed from different scale expansions, it is natural to try the method of matched asymptotic expansions [17]. If there is an overlap region where both approximations (post-Newtonian and tidal perturbation) are valid, a diffeomorphism can be constructed between charts used in different regions of the manifold by different approximation schemes. Matching—demanding that both approximation schemes have the same asymptotic form in the overlap region—relates physical observables in the different regions, *i.e.* ensures that both expansions represent the same physical system.

The first attempt to construct initial data in such a way was by Alvi [18]. By construction, there are discontinuities in the data, which were found to be too large for numerical experiments [19]. Alvi’s fundamental problem was that he did not match—construct expansions asymp-

totic to each other anywhere in the overlap region—but rather patched—set solutions equal to each other on specified 2-surfaces—so that large discontinuities in the extrinsic curvature were possible. In fact, inspection of Alvi’s Table I shows that his spatial metric near the black holes is discontinuous apart from the Minkowski terms (independent of G) in either region. Such discontinuities are problematic for numerical relativity, since part of the initial data is the extrinsic curvature which includes derivatives of the spacetime metric. Furthermore, construction of the extrinsic curvature requires terms in the expansions that Alvi did not calculate because the counting of orders does not follow the standard post-Newtonian pattern.

In this paper, we correct the mathematical problems with Alvi’s approach and provide initial data for actual numerical evolutions. We use true asymptotic matching to construct a piecewise metric for two black holes in circular orbit, including terms of order the gravitational constant G on the diagonal of the metric and $O(G)^{3/2}$ (for a bound system) off the diagonal. We also remove the piecewise nature of the approximate metric by “merging” the solutions in different regions, thus generating a uniform approximate metric. We do this by constructing smooth transition functions so that the uniform approximate solution is in principle C^∞ , although in practice higher-order derivatives will be less accurate than lower-order ones. This metric allows for the calculation of the lapse to $O(G)$, the shift to $O(G)^{3/2}$, and the extrinsic curvature to $O(G)^{3/2}$. Although this data contains only the first order deviations from flat spacetime, our approach does include deviations from conformal flatness encoded in the tidal perturbations near the black holes. In principle, this initial data formally satisfies the constraints only up to the same order as the errors in the approximate metric, and hence it might still need to be projected to the constraint hypersurface via a conformal decomposition. Nonetheless, since the constraint violations are $O(G)^{3/2}$ or smaller, we expect any reasonable constraint projection algorithm to change the physical content of our initial data only at a comparably small order. In conclusion, we develop a general formalism to construct astrophysically realistic initial data that can be extended to higher order by including more precise post-Newtonian [20] and black hole perturbation theory results [21] already in the literature.

This paper is organized as follows: Sec. II explains the general formalism of matched asymptotic expansions as applicable to numerical relativity. Sec. III describes the approximation regions, the orders of the approximations, and their errors. Sec. IV discusses the near zone expansion of the metric and determines its asymptotic expansion in the overlap region. Sec. V concentrates on the inner zone solution and expands it asymptotically in the overlap region. Sec. VI applies asymptotic matching to the metrics to obtain matching relations between expansion coefficients and a map that relates the charts used in the different regions. Sec. VII constructs the

global metric, discusses its properties, and builds transition functions to eliminate discontinuities between local approximations. Sec. VIII computes the extrinsic curvature, lapse and shift. Sec. IX concludes and points toward future research.

Throughout this paper we use geometrized units ($G = c = 1$). We use the tilde as a relational symbol such that $a \sim b$ means “ a is asymptotic to b ” [17]. We refer to our matched solutions as global. Strictly speaking, our final matched asymptotic expansion is not good out in the radiation zone (further from the binary than a reduced wavelength of the gravitational waves). However, that part of the solution and its matching to the part we do consider are solved problems [15]. Thus our solutions could straightforwardly be made global, and in any event they cover the region within a reduced wavelength of the binary which is of most interest to numerical relativity.

II. ASYMPTOTIC MATCHING IN GENERAL RELATIVITY

The theory of matched asymptotic expansions was first developed to perform multiple scale analysis on non-linear partial differential equations to obtain global approximate solutions [17]. In general relativity, this method was first applied by Burke and Thorne [22], Burke [23], and D’Eath [24, 25] in the 1970s to derive corrections to the laws of motion due to coupling of the body’s motion to the geometry of the surrounding spacetime. Based on these ideas, this section develops a version of the theory of matched asymptotics that is useful to obtain initial data for numerical relativity simulations.

Consider a manifold $(\mathcal{M}, g_{\mu\nu})$, that can be divided into n closed subsets \mathcal{C}_n with $n \geq 2$. Technically these subsets are submanifolds of the same dimensionality as \mathcal{M} . Each of these submanifolds, endowed with its own chart and metric, overlaps with its adjacent neighbors in some 4-volume that is not the empty set; *i.e.* $\mathcal{C}_n \cap \mathcal{C}_m = \mathcal{O}_{nm}$ where the overlap submanifolds \mathcal{O}_{nm} are also closed. In particular, we will consider cases in which these overlap submanifolds are closed and bounded, so that they are actually compact. If we choose a spatial hypersurface in these manifolds, then the overlap submanifolds (4-volumes) become overlap hypersurfaces (3-volumes).

We assume that on each \mathcal{C}_n there exists a well-defined approximate solution to the Einstein equations for some specific physical scenario. In other words, even though there is an unknown unique metric on the manifold (a global solution to the differential system posed by the physics), each submanifold will have its own approximate version. This approximate metric will be locally valid on that subset and will depend on parameters native to that submanifold.

In general, the approximate metric solution valid on the n th submanifold can be expressed as

$$g_{\mu\nu}^{(n)} = g_{\mu\nu}^{(n) \text{ background}} + g_{\mu\nu}^{(n) \text{ perturbation}}, \quad (1)$$

where $g_{\mu\nu}^{perturbation} \ll g_{\mu\nu}^{background}$. For example, in a post-Minkowskian expansion, $g_{\mu\nu}^{background} = \eta_{\mu\nu}$, where $\eta_{\mu\nu}$ is the flat metric, while in black hole perturbation theory $g_{\mu\nu}^{background} = g_{\mu\nu}^{Schwarzschild}$, where $g_{\mu\nu}^{Schwarzschild}$ is the metric for a Schwarzschild black hole. Furthermore, in each \mathcal{C}_n the perturbative solution $g_{\mu\nu}^{(n) perturbation}$ is expanded in some coordinate-dependent local parameter $\epsilon_{(n)} \ll 1$. For example, in post-Newtonian theory the expansion parameter is $\epsilon_{PN} = m_A/r_A$, where m_A is the mass of body A and r_A is the distance from it to the field point. In this approximation scheme, the distance r_A is assumed larger than the radius \mathcal{R} of spacetime curvature, so that $r_A \gg \mathcal{R}$, and $g_{\mu\nu}^{(n) perturbation}$ can be expanded in ϵ_{PN} [16].

The overlap subset \mathcal{O}_{nm} can be characterized as a region where both $\epsilon_{(n)}$ and $\epsilon_{(m)}$ are small. These small parameters will be dimensionless, depending on both coordinates and some inherent scales locally defined in \mathcal{C}_n and \mathcal{C}_m . In general, in order to guarantee the existence of an overlap set, these parameters must take the form

$$\epsilon_{(n)} = \left[\frac{s_{(n)}}{R(x_{(n)}^\mu)} \right]^p, \quad \epsilon_{(m)} = \left[\frac{R(x_{(m)}^\mu)}{s_{(m)}} \right]^p, \quad (2)$$

where $s_{(n,m)}$ are local scale measures, $R(x_{(n,m)}^\mu)$ are functions of the coordinates and $p \in \mathbb{R}$. In Eq. (2) $s_{(m)}$ gives the scale for the outer boundary of \mathcal{O}_{nm} , while $s_{(n)}$ gives the scale for the inner boundary, so that $s_{(n)} \ll s_{(m)}$. Since these parameters must be smaller than one, we obtain a measure of the extent (boundedness) of the overlap subset, *i.e.*

$$s_{(m)} \ll R(x^\mu) \ll s_{(n)}. \quad (3)$$

If there are n submanifolds \mathcal{C}_n and $n-1$ overlap regions \mathcal{O}_{nm} , there will be n approximate solutions, where the n th solution on the n th submanifold could be expressed as

$$g_{\mu\nu}^{(n)} \sim \sum_{l=0}^{l=L} F_{\mu\nu}^{(n)} \epsilon_{(n)}^l. \quad (4)$$

In Eq. (4), $\epsilon_{(n)}$ is a small dimensionless parameter that depends on at least one coordinate defined in \mathcal{C}_n . On the other hand, the $F_{\mu\nu}^{(n)}$ are functions that do not depend on the same coordinate as $\epsilon_{(n)}$, but that can depend on all other coordinates and on a set of parameters $\Theta_{(n)}^a$, which are also defined locally on \mathcal{C}_n . The $\Theta_{(n)}^a$ are related to physical parameters such as the masses of the holes, but such identifications are inherently imprecise in asymptotic matching [16].

In general, approximate metrics of the type of Eq. (4) will be expansions that will depend on coordinates and parameters local only to the submanifold where the solution is valid. Asymptotic matching provides a diffeomorphism and matching conditions to relate coordinates and

parameters that live in different submanifolds by comparing invariants in the overlap region.

If such an overlap subset \mathcal{O}_{nm} exists, then uniqueness theorems of asymptotic analysis [17] guarantee that the asymptotic expansions of adjacent approximations will be asymptotic to each other in \mathcal{O}_{nm} . Let us denote the asymptotic expansion in \mathcal{O}_{nm} of the solution valid in the n th submanifold with a tilde, so that

$$\tilde{g}_{\mu\nu}^{(n)} \sim \sum_{l=0}^L \sum_{k=0}^K \epsilon_{(n)}^l \epsilon_{(m)}^k G_{\mu\nu}^{(n)}, \quad (5)$$

where $G_{\mu\nu}^{(n)}$ is a new set of functions obtained by expanding $F_{\mu\nu}^{(n)}$ in the overlap region \mathcal{O}_{nm} as a series in $\epsilon_{(m)} \ll 1$, where this parameter is small inside the overlap region. Similarly, let us denote the asymptotic expansion in \mathcal{O}_{nm} of the solution valid in the m th submanifold by

$$\tilde{g}_{\mu\nu}^{(m)} \sim \sum_{l=0}^L \sum_{k=0}^K \epsilon_{(m)}^k \epsilon_{(n)}^l G_{\mu\nu}^{(m)}, \quad (6)$$

This time $G_{\mu\nu}^{(m)}$ is an expansion of $F_{\mu\nu}^{(m)}$ inside \mathcal{O}_{nm} in terms of $\epsilon_{(n)}$, which is also small in the overlap region. Note that the asymptotic expansions in \mathcal{O}_{nm} (Eqs. (5) and (6)) are bivariate, *i.e.* depend on two independent expansion parameters $\epsilon_{(n)}$ and $\epsilon_{(m)}$. These asymptotic expansions are valid in \mathcal{O}_{nm} because the expansion parameters are not only small in their respective subsets (\mathcal{C}_n and \mathcal{C}_m), but they are also small in the intersection of these subsets, \mathcal{O}_{nm} , where $\mathcal{O}_{nm} \subset \mathcal{C}_m$ and $\mathcal{O}_{nm} \subset \mathcal{C}_n$.

Now that the asymptotic expansions of the approximate solutions on the n th and m th submanifolds have been found inside the overlap region \mathcal{O}_{nm} , we must require that line elements computed with the asymptotic adjacent metrics ($\tilde{g}_{\mu\nu}^{(n)}$ and $\tilde{g}_{\mu\nu}^{(m)}$) be asymptotic to each other. In terms of the metrics, we have the condition

$$\tilde{g}_{\mu\nu}^{(n)}(x_{(n)}^\sigma) \sim \frac{\partial x_{(m)}^\rho}{\partial x_{(n)}^\mu} \frac{\partial x_{(m)}^\lambda}{\partial x_{(n)}^\nu} \tilde{g}_{\rho\lambda}^{(m)}(x_{(m)}^\sigma(x_{(n)}^\sigma)). \quad (7)$$

Since the two metrics have the asymptotic forms (5) and (6), Eq. (7) implies that the coordinates and parameters must also be asymptotic to each other. In other words, the diffeomorphism and parameter matching must take the form

$$\begin{aligned} x_{(m)}^\sigma &= x_{(n)}^\sigma \sum_{j=0}^J \left(\frac{s_{(n)}}{s_{(m)}} \right)^j \chi_{\sigma j}, \\ \Theta_{(m)}^a &= \Theta_{(n)}^a \sum_{j=0}^J \left(\frac{s_{(n)}}{s_{(m)}} \right)^j \kappa_{aj}. \end{aligned} \quad (8)$$

where the $\chi_{\sigma j}$ stands for a matrix of unknown functions (a different function per coordinate per order), and where κ_{aj} is also a matrix of unknown coordinate-independent

coefficients (a different coefficient per matching parameter per order). The coordinate transformation postulated in Eq. (8) is really a bivariate asymptotic expansion, where all $\chi_{\sigma j}$ are series in $\epsilon_{(m)}$ that do not depend on $\epsilon_{(n)}$. Also note that the matching conditions postulated are coordinate independent, because the fraction $s_{(n)}/s_{(m)}$ depends only on scales and the matrix κ_{aj} contains only coordinate-independent coefficients.

Using Eq. (8) in Eq. (7), we obtain J sets of 10 partial differential equations per overlap patch that can now be solved, obtaining a diffeomorphism ϕ_{nm} and matching conditions ψ_{mn} that relate coordinates and parameters inherent to \mathcal{C}_n to those local to \mathcal{C}_m . If there are N such overlap patches, then with this procedure we obtain $N J$ sets of 10 partial differential equations, that when solved provide a collection of maps $\{\phi_{nm}\}$ and matching conditions $\{\psi_{nm}\}$ for the entire atlas of \mathcal{M} .

The diffeomorphisms and matching conditions allow for an approximate expression of the global metric as a piecewise function (one defined on non-overlapping manifolds), such as

$$g_{\mu\nu} \approx \begin{cases} \frac{\partial x_{(0)}^{\mu'}}{\partial x_{(n)}^{\mu}} \frac{\partial x_{(0)}^{\nu'}}{\partial x_{(n)}^{\nu}} \dots g_{\mu'\nu'}^{(0)}(x_{(n)}^{\alpha}; \Theta_{(n)}^a), & \text{in } \mathcal{C}_0 \\ \frac{\partial x_{(1)}^{\mu'}}{\partial x_{(n)}^{\mu}} \frac{\partial x_{(1)}^{\nu'}}{\partial x_{(n)}^{\nu}} g_{\mu'\nu'}^{(1)}(x_{(n)}^{\alpha}; \Theta_{(n)}^a), & \text{in } \mathcal{C}_1 \setminus \mathcal{C}_0 \\ \vdots \\ g_{\mu\nu}^{(n)}(x_{(n)}^{\alpha}; \Theta_{(n)}^a), & \text{in } \mathcal{C}_n \setminus \dots \setminus \mathcal{C}_1 \setminus \mathcal{C}_0, \end{cases} \quad (9)$$

where we have explicitly transformed all metrics to the coordinate system of the n th chart. Equation (9) and all of its derivatives are discontinuous on the boundaries between non-overlapping manifolds, with discontinuities of the order of the errors in the local approximations. For example, if the asymptotic expansions of the metric in each \mathcal{O}_{nm} have errors of $O(\epsilon_{(n)})^L$ or $O(\epsilon_{(m)})^K$, then the discontinuities at the boundary, wherever it is chosen in \mathcal{O}_{nm} , are of the same order.

III. APPROXIMATION REGIONS AND PRECISION

Let us consider a binary black hole spacetime, where the manifold (Fig. 1) is divided into 4 submanifolds, the boundaries of which cannot be determined precisely without knowing the radii of convergence of the black hole perturbation theory (BHPT) and post-Newtonian (PN) asymptotic series:

1. **The inner zone of Black Hole 1**, (submanifold \mathcal{C}_1): $R_1 \ll b$, where R_A is the distance from the A th black hole in isotropic coordinates centered on black hole 1 (BH1), and b is the distance between the two black holes. In this region, the metric is obtained via black hole perturbation theory as an expansion in $\epsilon_{(1)} = R_1/b$. [16, 18].

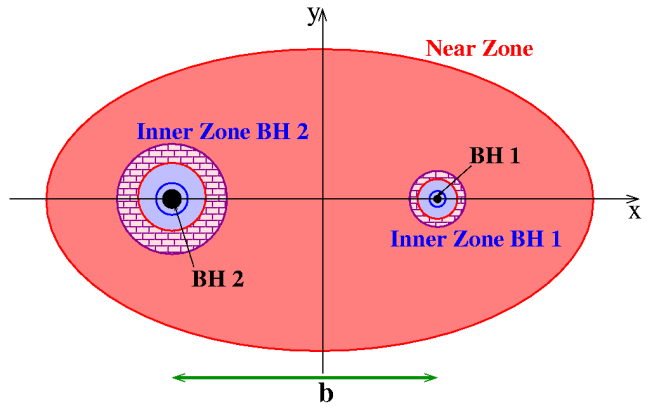


FIG. 1: Schematic diagram of the near zone (red or dark gray), inner zones (blue or light gray) and buffer zones (checkered pink). The near zone extends up to the inner boundary of the buffer zone, while the inner zone extends from the outer boundary of the buffer zone up to the black hole. Therefore, the buffer zone is an annulus where both the near zone and inner zones overlap. BH1 and BH2 (black) are separated by a distance b .

2. **The inner zone of Black hole 2**, (submanifold \mathcal{C}_2): $R_2 \ll b$, where the metric is obtained in the same manner as in region 1 but with labels 1 and 2 swapped (and the isotropic coordinates are centered on black hole 2 (BH2)).
3. **The near zone**, (submanifold \mathcal{C}_3): $r_A \gg m_A$ and $r \leq \lambda/2\pi$, where λ is the wavelength of gravitational radiation, r is the distance from the binary center of mass in harmonic coordinates, and $r_A - m_A$ is the separation in harmonic coordinates from the horizon of the A th black hole (which has mass m_A). In this region, a post-Newtonian approximation is used for the metric with an expansion parameter $\epsilon_{(3)} = m_A/r_A$ [15] which is formally treated as the same order for both values of A .
4. **The far zone**, (submanifold \mathcal{C}_4): $r \geq \lambda/2\pi$, where the metric is obtained from a post-Minkowski calculation [26].

For asymptotic matching to be possible, there must exist a 4-volume where adjacent regions overlap, which is referred to as the buffer zone or overlap region. There exist three such \mathcal{O}_{nm} : two (\mathcal{O}_{13} and \mathcal{O}_{23}) overlap the near zone and the inner zones of black hole 1 and 2; the third one occurs between the near and the radiation zones (\mathcal{O}_{34}). The former, which is shown in Fig. 1, leads to the asymptotic condition $m_A \gg r_A \gg b$, while the latter case (not shown in the figure), has been analyzed in Ref. [15], and will not be discussed here. In this paper we match asymptotic expansions in the near zone and the two inner zones.

In order to perform asymptotic matching it is necessary to asymptotically expand the two adjacent metrics in the overlap regions. In other words, the inner zone line

elements must be asymptotically expanded in powers of $\epsilon_{(1,2)}$, while the near zone must be expanded in powers of $\epsilon_{(3)}$. The resulting metrics are bivariate expansions, since they depend on two *independent* perturbation parameters $\epsilon_{(1,2)}$ and $\epsilon_{(3)}$. Care must be taken when performing these expansions, because each must be taken to the same bivariate order $O(\epsilon_{1,2}^q \epsilon_3^p)$.

Since we expand in two small quantities, we write order symbols with multiple arguments. A term of $O(p, q)$ means it is of order $(m/b)^p (r_A/b)^q$. However, when we write remainders the meaning of the symbol is slightly different: a remainder of $O(p, q)$ means that terms of order $(m/b)^p$ or $(r_A/b)^q$ are neglected.

By comparing the asymptotic expansions of the inner and near zones in the buffer region, asymptotic matching will provide a coordinate transformation and a parameter matching relationship. In this manner, a global uniform metric is generated for all regions in the form of a piecewise function. Due to the inherent piecewise nature of the global solution, one must choose a 2-surface, for example a fixed radius r^M , inside the overlap region, where two adjacent solutions are joined together. There is an infinite number of such 2-surfaces, since the overlap region exists as a 4-volume. There will exist small discontinuities at the chosen 2-surface that should be controllable by the size of the perturbation parameters. Nonetheless, if the perturbation parameters are chosen small enough, these errors can become as small as desired, and in particular, smaller than numerical resolution.

The optimum 2-surface would be that in which the errors of the approximations in the inner zone and near zone approach each other's size asymptotically. For example, for the overlap region near black hole 1, we will see in the next section that the error in the inner zone scales as $(m_2/b)(R_1/b)^3$, and the error in the near zone scales as $(m_1/r_1)^2$. These errors lead to the asymptotic condition

$$r_1^M \propto \left(\frac{m_1^2 b^4}{m_2} \right)^{1/5}. \quad (10)$$

where we can fix the constant of proportionality with an arbitrary function β , so that

$$r_1^M \sim \left(\beta(m, b) \frac{m_1^2 b^4}{m_2} \right)^{1/5}. \quad (11)$$

It is clear, however, that some conditions must be imposed on $\beta(m, b)$, since r^M cannot be inside the event horizon of either black hole. Imposing these conditions leads to

$$\frac{m_2 b}{m_1^2} \gg \beta(m, b) \gg \frac{m_1^3 m_2}{b^4}. \quad (12)$$

This function $\beta(m, b)$ explicitly shows the freedom that exists in asymptotic matching since we can shift r^M inside the buffer region at will, as long as we respect that $m \ll r^M \ll b$.

Finally, we enumerate the orders of approximation used in the near zone. The Einstein equations are guaranteed to generate a well-posed initial value problem for globally hyperbolic spacetimes [1], where the initial data could consist of the extrinsic curvature K_{ij} and the spatial 3-metric $\gamma_{ij} = g_{ij}$. We can write the extrinsic curvature in the form

$$K_{ij} = \frac{1}{2\alpha} (2D_{(i}\beta_{j)} - \partial_t \gamma_{ij}), \quad (13)$$

where $\beta_i = g_{0i}$ is the shift vector and α is the lapse. Time derivatives are smaller than spatial derivatives by a characteristic velocity, which by the virial theorem is $O(m/b)^{1/2}$. Therefore to compute K_{ij} consistently to a given order in m/b , the 4-metric components g_{0i} are needed to $O(m/b)^{1/2}$ beyond the highest order in g_{ij} (and g_{00} , which appears in α). In this paper we compute the first non-Minkowski contributions to the 3-metric and extrinsic curvature, which means that we need the 4-metric components g_{00} and g_{ij} to $O(m/b)$, but we need g_{0i} to $O(m/b)^{3/2}$. Note that this does not correspond to any standard post-Newtonian order counting or nomenclature, which is why we quote precisions and remainders precisely in terms of expansion parameters rather than in ambiguous terms such as “nth PN”.

IV. NEAR ZONE METRIC

In this section, we present the post-Newtonian (PN) metric in the near zone \mathcal{C}_3 and expand it in the buffer zone \mathcal{O}_{13} , between the inner zone of BH1 and the near zone. Due to the symmetry of the problem, it suffices to do the matching in just one overlap region. Matching for the other overlap region \mathcal{O}_{23} will be given by a symmetry transformation in later sections.

We use harmonic corotating coordinates (t, x, y, z) such that

$$\begin{aligned} t' &= t, \\ x' &= x \cos \omega t - y \sin \omega t, \\ y' &= x \sin \omega t + y \cos \omega t, \\ z' &= z, \end{aligned} \quad (14)$$

where primes stand for harmonic coordinates and unprimed symbols corresponds to the corotating harmonic coordinates with origin at the center of mass. Note that in this coordinate system the event horizon is located at $r_{1,2} = m_{1,2}$. The near-zone metric takes the form [27]

$$\begin{aligned} g_{00}^{(3)} &\approx -1 + \frac{2m_1}{r_1} + \frac{2m_2}{r_2} + \omega^2(x^2 + y^2), \\ g_{01}^{(3)} &\approx -y \omega \left(1 + \frac{2m_1}{r_1} \right), \\ g_{02}^{(3)} &\approx x \omega \left(1 + \frac{2m_1}{r_1} \right) - 4\mu b \omega \left(\frac{1}{r_1} - \frac{1}{r_2} \right), \\ g_{ij}^{(3)} &\approx \delta_{ij} \left(1 + \frac{2m_1}{r_1} + \frac{2m_2}{r_2} \right), \end{aligned} \quad (15)$$

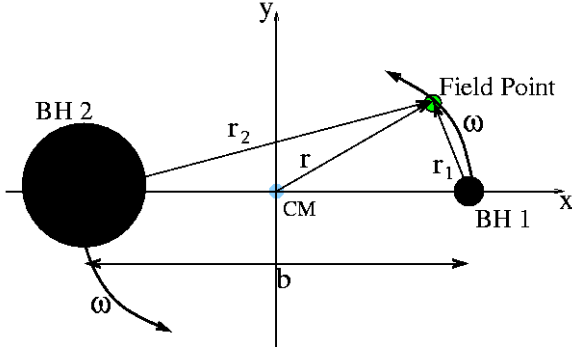


FIG. 2: Diagram of the near zone coordinate system. Observe that harmonic coordinates are measured with origin at the center of mass, but r_1 and r_2 are measured from black holes 1 and 2 respectively. Also note that the black holes are rotating in the counter clockwise direction. From this diagram it is also clear that $\vec{r}_2 = \vec{r}_1 + \vec{b}$.

where all remainders are $O(m/r)^2$ and the superscript reminds us we are working on submanifold \mathcal{C}_3 . Implicit in this metric is the assumption that r_A is of order b , or in other words that we are not too close to one of the holes. Note that we do not include the $O(m/r)^2$ terms in g_{00} in what is commonly called the first post-Newtonian (1PN) metric and that we do include $O(m/r)^{3/2}$ terms in g_{0i} .

In Eq. (15), the angular velocity is defined by

$$\omega = \sqrt{m/b^3} \left[1 + \left(3 - \frac{\mu}{m} \right) \frac{m}{b} \right], \quad (16)$$

where we have included the PN corrections to the Keplerian angular velocity of $O(m/b)$, $\mu = m_1 m_2 / (m_1 + m_2)$ is the reduced mass of the system, and b is the coordinate distance between the two black holes.

Also $r_A - m_A$ refers to the separation in harmonic coordinates from the horizon of the A th black hole,

$$\begin{aligned} r_1 &= \sqrt{x_1^2 + y^2 + z^2} = \sqrt{(x - m_2 b/m)^2 + y^2 + z^2}, \\ r_2 &= \sqrt{x_2^2 + y^2 + z^2} = \sqrt{(x + m_1 b/m)^2 + y^2 + z^2}, \end{aligned} \quad (17)$$

so that $\vec{r}_2 = \vec{r}_1 + \vec{b}$, where $\vec{b} = b \hat{x}_2$, points from black hole 2 to 1, as shown in Fig. 2.

We now concentrate on the overlap region (buffer zone) \mathcal{O}_{13} . Inside \mathcal{O}_{13} we can expand all terms proportional to $1/r_2$ in Legendre polynomials of the form

$$\frac{1}{r_2} = \frac{1}{b} \sum_{n=0}^{\infty} (-1)^n \left(\frac{r_1}{b} \right)^n P_n \left(\frac{x_1}{r_1} \right). \quad (18)$$

Substituting into Eq. (15), we obtain

$$\begin{aligned} \tilde{g}_{00}^{(3)} &\sim -1 + \frac{2m_1}{r_1} + \frac{2m_2}{b} \left[1 - \frac{r_1}{b} P_1 \left(\frac{x_1}{r_1} \right) + \left(\frac{r_1}{b} \right)^2 P_2 \left(\frac{x_1}{r_1} \right) \right] + \omega^2 (x^2 + y^2), \\ \tilde{g}_{01}^{(3)} &\sim -y \omega \left\{ 1 + \frac{2m_1}{r_1} + \frac{2m_2}{b} \left[1 - \frac{r_1}{b} P_1 \left(\frac{x_1}{r_1} \right) \right] \right\}, \\ \tilde{g}_{02}^{(3)} &\sim x \omega \left\{ 1 + \frac{2m_1}{r_1} + \frac{2m_2}{b} \left[1 - \frac{r_1}{b} P_1 \left(\frac{x_1}{r_1} \right) \right] \right\} - 4\mu b \omega \left\{ \frac{1}{r_1} - \frac{1}{b} \left[1 - \frac{r_1}{b} P_1 \left(\frac{x_1}{r_1} \right) + \left(\frac{r_1}{b} \right)^2 P_2 \left(\frac{x_1}{r_1} \right) \right] \right\}, \\ \tilde{g}_{03}^{(3)} &\sim O(2, 3), \\ \tilde{g}_{ij}^{(3)} &\sim \delta_{ij} \left\{ 1 + \frac{2m_1}{r_1} + \frac{2m_2}{b} \left[1 - \frac{r_1}{b} P_1 \left(\frac{x_1}{r_1} \right) + \left(\frac{r_1}{b} \right)^2 P_2 \left(\frac{x_1}{r_1} \right) \right] \right\}, \end{aligned} \quad (19)$$

where all errors are of order $O(2, 3)$ and where $m_1 \ll r \ll b$. The metric (19), denoted with a tilde, is the asymptotic expansion in the inner zone of BH1 of the PN metric, which is already an asymptotic expansion in the near zone.

Observe that these expansions constitute a series within a series (bivariate series). In order to see this

more clearly, we can rearrange the spatial metric to get

$$\begin{aligned} \tilde{g}_{ij}^{(3)} &\sim \delta_{ij} \left(1 + \frac{2m_1}{r_1} \left\{ 1 + \frac{m_2}{m_1} \frac{r_1}{b} \left[1 - \frac{r_1}{b} P_1 \left(\frac{x_1}{r_1} \right) + \left(\frac{r_1}{b} \right)^2 P_2 \left(\frac{x_1}{r_1} \right) \right] \right\} \right), \\ m_1 &\ll r_1 \ll b. \end{aligned} \quad (20)$$

Equation (20) is a generalized Frobenius series [28], where the expansion is about the regular singular points $r_1 = 0$ and $r_1 = \infty$. There are clearly two independent perturbation parameters, namely $\epsilon_{(3)} = m_1/r_1$, the usual PN expansion parameter valid in \mathcal{C}_3 , and a tidal perturbation

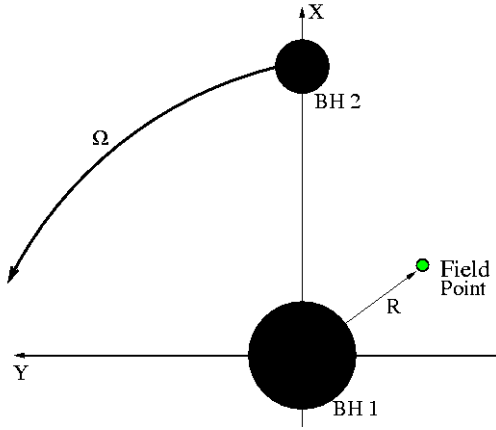


FIG. 3: Coordinate system used in the inner zone. In isotropic coordinates, the origin is at black hole 1 and the other hole orbits around with angular velocity Ω . The matching parameters M_1 and Ω and the coordinates X^μ will not be equal to those used in the near zone.

parameter, $\epsilon_{(1)} = r_1/b$, valid in the overlap region \mathcal{O}_{13} .

V. INNER ZONE METRIC

In this section we discuss the metric in the inner zone \mathcal{C}_1 of BH1 and its asymptotic expansion in the overlap region \mathcal{O}_{13} .

Physically, we expect the spacetime in the inner zone of BH1 to be Schwarzschild with mass M_1 plus a tidal perturbation due to BH2. Thorne and Hartle [16] argue that, in the local asymptotic rest frame (LARF) of BH1, the metric can be expanded in powers of M_1 outside the

horizon of BH1. The first term, independent of M_1 , can be taken to represent the external universe and thus can be computed by placing a test particle in the spacetime of BH2 as done by Alvi [18]. This is the tidal perturbation due to BH2. Terms of higher order in M_1 describe BH1 itself (the Schwarzschild metric) and interactions between BH1 and BH2 (tidally-induced quadrupole, etc). At the level of approximation of this paper, we can neglect the interaction terms because they are $O(2, 1)$ or higher.

Alvi identifies LARF coordinates, in terms of which the tidal perturbation is obtained, with isotropic coordinates (Fig. 3). Observe that this coordinate system is centered on BH1 and is inertial (includes no rotation). Alvi's identification only makes sense in the buffer zone—for example, there is no horizon around a test particle—which becomes important when we examine the metric below. The asymptotic form of the tidally perturbed metric valid in the buffer zone is given by Eq. (3.14) of Ref. [18].

But what about the perturbation in the part of the inner zone not in the buffer zone, *i.e.* in the strong-field region of BH1? Due to the nonlinearity of the Einstein equations, a linear superposition of solutions (Schwarzschild plus tides) is in general not another solution. Thus summing the full Schwarzschild metric plus the perturbation terms in Eq. (3.14) of Ref. [18] would not give a valid perturbation in the strong-field part of the inner zone. Instead, Alvi [18] guesses a functional form of the inner zone metric and shows that it does solve the Einstein equations to first order in the tidal perturbation. The result is given in his Eq. (3.23) and depends on parameters M_1 and Ω which will be related to the near-zone parameters m_1 and ω when we perform the matching.

We write Eq. (3.23) of Ref. [18] as

$$\begin{aligned}
h_{00}^{IC,(1)} &\approx -\left[\frac{1-M_1/(2R_1)}{1+M_1/(2R_1)}\right]^2 + \frac{m_2}{b^3}\left(1-\frac{M_1}{2R_1}\right)^4 \left[3(X\cos\Omega T + Y\sin\Omega T)^2 - R_1^2\right], \\
h_{01}^{IC,(1)} &\approx \frac{2m_2}{b^3}\sqrt{\frac{m}{b}}\left(1-\frac{M_1}{2R_1}\right)^2\left(1+\frac{M_1}{2R_1}\right)^4 \left[(Z^2 - Y^2)\sin\Omega T - XY\cos\Omega T\right], \\
h_{02}^{IC,(1)} &\approx \frac{2m_2}{b^3}\sqrt{\frac{m}{b}}\left(1-\frac{M_1}{2R_1}\right)^2\left(1+\frac{M_1}{2R_1}\right)^4 \left[(X^2 - Z^2)\cos\Omega T + XY\sin\Omega T\right], \\
h_{03}^{IC,(1)} &\approx \frac{2m_2}{b^3}\sqrt{\frac{m}{b}}\left(1-\frac{M_1}{2R_1}\right)^2\left(1+\frac{M_1}{2R_1}\right)^4 (Y\cos\Omega T - X\sin\Omega T) Z, \\
h_{ij}^{IC,(1)} &\approx \left(1+\frac{M_1}{2R_1}\right)^4 \left(\delta_{ij} + \frac{m_2}{b^3} \left[3(X\cos\Omega T + Y\sin\Omega T)^2 - R_1^2\right] \left\{ \left[\left(1+\frac{M_1}{2R_1}\right)^4 - \frac{2M_1^2}{R_1^2}\right] \delta_{ij} \right. \right. \\
&\quad \left. \left. - \frac{2M_1}{R_1} \left(1+\frac{M_1^2}{4R_1^2}\right) \frac{X^i X^j}{R_1^2} \right\} \right), \tag{21}
\end{aligned}$$

where once more the numerical superscript is to remind

us that this metric is valid in submanifold \mathcal{C}_1 , while the

IC superscript refers to isotropic coordinates. The remainders in Eq. (21) are $O(R_1/b)^3$.

Inspection of Eq. (21) shows that the perturbed metric diverges as $R_1 \rightarrow 0$ faster than $(1/R_1)^4$. This looks like a problem since the perturbation then dominates the Schwarzschild background as $R_1 \rightarrow 0$, which prevents the use of a puncture trick [10] to avoid excising the black hole interior when projecting onto the constraint manifold. The problem arises because Alvi [18] identified the LARF coordinates of the perturbation with isotropic coordinates of a Schwarzschild black hole. However, the tidal perturbation tacitly assumes a small space-like separation from the event horizon. Since $R_1 \rightarrow 0$ in isotropic coordinates corresponds to spacelike infinity in the causally disconnected region of the Kruskal diagram, the perturbation of course diverges. (Thus the identification of LARF coordinates with isotropic coordinates only makes sense in the buffer zone.) In a later paper [29] Alvi tries to avoid the $R_1 \rightarrow 0$ problem by performing a transformation from isotropic coordinates to ingoing Eddington-Finkelstein coordinates. However, practical numerical evolutions will excise inside the horizon, and thus the use of ingoing coordinates is unnecessary since the $R_1 \rightarrow 0$ behavior is avoided anyway.

Since matching will be simpler if performed between two coordinate systems that live in charts that are similar to each other, we choose to corotate first. We define inner isotropic corotating coordinates (ICC)

$$\begin{aligned}\bar{X} &= X \cos \Omega T + Y \sin \Omega T, \\ \bar{Y} &= -X \sin \Omega T + Y \cos \Omega T, \\ \bar{Z} &= Z, \\ \bar{T} &= T.\end{aligned}\tag{22}$$

From these equations, we can apply a gauge transformation to obtain the inner metric in inner isotropic corotating coordinates, given by

$$\begin{aligned}h_{00}^{(1)} &\approx H_t + H_{s1}\Omega^2 (\bar{X}^2 + \bar{Y}^2) \\ &\quad + 2H_{st}\bar{X}\frac{\Omega}{b^2} (\bar{X}^2 + \bar{Y}^2 - \bar{Z}^2), \\ h_{11}^{(1)} &\approx H_{s1} - H_{s2}\frac{\bar{X}^2}{b^2}, \\ h_{01}^{(1)} &\approx -H_{s1}\bar{Y}\Omega - H_{st}\frac{\bar{Y}\bar{X}}{b^2}, \\ h_{22}^{(1)} &\approx H_{s1} - H_{s2}\frac{\bar{Y}^2}{b^2}, \\ h_{02}^{(1)} &\approx H_{s1}\bar{X}\Omega + \frac{H_{st}}{b^2} (\bar{X}^2 - \bar{Z}^2), \\ h_{33}^{(1)} &\approx H_{s1} - H_{s2}\frac{\bar{Z}^2}{b^2}, \\ h_{03}^{(1)} &\approx H_{st}\frac{\bar{Y}\bar{Z}}{b^2}, \\ h_{12}^{(1)} &\approx -H_{s2}\frac{\bar{Y}\bar{X}}{b^2}, \\ h_{23}^{(1)} &\approx -H_{s2}\frac{\bar{Z}\bar{Y}}{b^2}, \\ h_{13}^{(1)} &\approx -H_{s2}\frac{\bar{Z}\bar{X}}{b^2},\end{aligned}\tag{23}$$

where we use the shorthand

$$\begin{aligned}H_{st} &= 2m_2\omega \left(1 - \frac{M_1}{2R_1}\right)^2 \left(1 + \frac{M_1}{2R_1}\right)^4, \\ H_{s1} &= \left(1 + \frac{M_1}{2R_1}\right)^4 \left\{1 + 2\frac{m_2}{b^3}R_1^2P_2\left(\frac{\bar{X}}{R_1}\right) \left[\left(1 + \frac{M_1}{2R_1}\right)^4 - 2\frac{M_1^2}{R_1^2}\right]\right\}, \\ H_{s2} &= \left(1 + \frac{M_1}{2R_1}\right)^4 \left(1 + \frac{M_1^2}{4R_1^2}\right) \frac{4m_2M_1}{bR_1} P_2\left(\frac{\bar{X}}{R_1}\right), \\ H_t &= -\left(\frac{1 - M_1/2R_1}{1 + M_1/2R_1}\right)^2 + 2\left(1 - \frac{M_1}{2R_1}\right)^4 \frac{m_2}{b^3}R_1^2P_2\left(\frac{\bar{X}}{R_1}\right),\end{aligned}\tag{24}$$

and the errors are still $O(R_1/b)^3$. In Eq. (23) we have dropped the superscript ICC in favor of (1), which refers to submanifold \mathcal{C}_1 .

By expanding Eq. (23) in powers of M_1/R_1 , which is

permissible in overlap region \mathcal{O}_{13} , we obtain

$$\begin{aligned}\tilde{h}_{00}^{(1)} &\sim -1 + \frac{2M_1}{R_1} + \frac{2m_2}{b^3}R_1^2P_2\left(\frac{\bar{X}}{R_1}\right) \\ &\quad + \Omega^2 (\bar{X}^2 + \bar{Y}^2), \\ \tilde{h}_{01}^{(1)} &\sim \frac{-2m_2}{b^3}\sqrt{\frac{m}{b}}\bar{Y}\bar{X} - \bar{Y}\Omega\left(1 + \frac{2M_1}{R_1}\right), \\ \tilde{h}_{02}^{(1)} &\sim \frac{2m_2}{b^3}\sqrt{\frac{m}{b}}(\bar{X}^2 - \bar{Z}^2) + \bar{X}\Omega\left(1 + \frac{2M_1}{R_1}\right), \\ \tilde{h}_{03}^{(1)} &\sim \frac{2m_2}{b^3}\sqrt{\frac{m}{b}}\bar{Z}\bar{Y},\end{aligned}$$

where the errors are $O(2, 3)$. Like Eq. (19), $\tilde{h}_{\mu\nu}^{(1)}$ is a bivariate expansion in both $\epsilon_{(1)} = R_1/b$ (valid in the inner zone \mathcal{C}_1) and $\epsilon_{(3)} = M_1/R_1$ (valid in the buffer zone \mathcal{O}_{13}). In other words, it is the asymptotic expansion in the buffer zone to the asymptotic expansion in the inner zone.

VI. ASYMPTOTIC MATCHING

In this section, we concentrate on finding a matching condition (ψ_{13}) and a coordinate transformation (ϕ_{13}) that maps elements in subset \mathcal{C}_1 adapted to isotropic

corotating coordinates (ICC) \bar{X}^μ to elements in subset \mathcal{C}_3 adapted to harmonic corotating coordinates (HCC) x^μ . By comparing Eqs. (19) and (25) term by term and order by order, we can determine how their physical parameters are related and what is a coordinate transformation that takes inner isotropic corotating coordinates to corotating harmonic coordinates. In this manner, we will construct a global solution as a piecewise function.

We assume that the coordinates are asymptotic to each other and that they can be expanded in an implicit bivariate series as given by Eq. (8). Therefore, let the map $\psi_{13} : \bar{X}^\mu \rightarrow x^\mu$ be given by

$$\begin{aligned}\bar{X} &\approx \left(x - \frac{m_2 b}{m} \right) + x \left[\left(\frac{m_2}{b} \right)^{1/2} \chi_1(x^\mu) + \left(\frac{m_2}{b} \right) \chi_2(x^\mu) + \left(\frac{m_2}{b} \right)^{3/2} \chi_3(x^\mu) \right], \\ \bar{Y} &\approx y \left[1 + \left(\frac{m_2}{b} \right)^{1/2} \gamma_1(x^\mu) + \left(\frac{m_2}{b} \right) \gamma_2(x^\mu) + \left(\frac{m_2}{b} \right)^{3/2} \gamma_3(x^\mu) \right], \\ \bar{Z} &\approx z \left[1 + \left(\frac{m_2}{b} \right)^{1/2} \zeta_1(x^\mu) + \left(\frac{m_2}{b} \right) \zeta_2(x^\mu) + \left(\frac{m_2}{b} \right)^{3/2} \zeta_3(x^\mu) \right], \\ \bar{T} &\approx t \left[1 + \left(\frac{m_2}{b} \right)^{1/2} \tau_1(x^\mu) + \left(\frac{m_2}{b} \right) \tau_2(x^\mu) + \left(\frac{m_2}{b} \right)^{3/2} \tau_3(x^\mu) \right],\end{aligned}\quad (26)$$

where χ, γ, ζ and τ are functions of the harmonic corotating coordinates and do not depend on m/b (or equivalently ω), but are instead expansions in r_1/b . The error in the above coordinate transformation is $O(2, 3)$, where the $O(2, 0)$ error comes from the explicit truncation of the m/b expansion and the $O(0, 3)$ error comes from implicitly truncating the undetermined functions at that order. The first term in the \bar{X} equation corresponds to a shift in the center of mass in order to give the same origin to both coordinate systems.

In a similar manner, let us assume that the matching parameters are also identical to first order and independent of coordinates as in Eq. (8). Let ψ_{13} then be given by

$$\begin{aligned}M_1 &\approx m_1 \left[1 + \left(\frac{m_2}{b} \right)^{1/2} \eta_1 + \frac{m_2}{b} \eta_2 + \left(\frac{m_2}{b} \right)^{3/2} \eta_3 \right], \\ \Omega &\approx \omega \left[1 + \left(\frac{m_2}{b} \right)^{1/2} \kappa_1 + \frac{m_2}{b} \kappa_2 + \left(\frac{m_2}{b} \right)^{3/2} \kappa_3 \right],\end{aligned}\quad (27)$$

where the errors are $O(m/b)^2$. Note that in Eqs. (26) and (27) we have chosen to denote the unknown functions and coefficients corresponding to different coordinates or parameters by different Greek letters, instead of using the compact double-label notation introduced in Eq. (8).

Using ψ_{13} we can transform Eq. (25) to harmonic corotating coordinates and impose the matching condition of

Eq. (7),

$$\tilde{g}_{\mu\nu}^{(3)}(x^\gamma) \sim \tilde{h}_{\alpha\beta}^{(1)}(\bar{X}^\gamma(x^\gamma)) \frac{\partial \bar{X}^\alpha}{\partial x^\mu} \frac{\partial \bar{X}^\beta}{\partial x^\nu}. \quad (28)$$

Equation (28) provides 10 independent asymptotic relations per order, all of which must be satisfied simultaneously. Each asymptotic relation results in a first-order partial differential equation for the coordinate transformation, resulting in 10 integration constants per order. As we shall see, the form of these constants is such that they can be fixed by choosing a Poincaré transformation between the two coordinate systems. Therefore we are free to choose them, and will generally choose them to simplify the calculation.

Equation (28) must be solved iteratively in orders of $(m/b)^{1/2}$. Evaluating the nonzero components (the diagonals) of Eq. (28) at zeroth order in m/b , *i.e.* comparing Eqs. (19) and (25), provides no information, since it only asserts that at lowest order both metrics represent Minkowski spacetime. This is true for any matching formulation involving metrics of objects that would have asymptotically flat spacetimes in isolation.

The asymptotic relations given by evaluating Eqs. (19),

(25), and (28) at $O(m/b)^{1/2}$ are

$$\begin{aligned}\chi_1 &\sim -x\chi_{1,x}, & \zeta_1 &\sim -z\zeta_{1,z} \\ \gamma_1 &\sim -y\gamma_{1,y}, & \tau_1 &\sim -t\tau_{1,t}, \\ t\tau_{1,x} &\sim x\chi_{1,t}, & y\gamma_{1,t} - t\tau_{1,y} &\sim \left(\frac{m_2}{m}\right)^{1/2}, \\ t\tau_{1,z} &\sim z\zeta_{1,t}, & x\chi_{1,y} &\sim -y\gamma_{1,x}, \\ z\zeta_{1,x} &\sim -x\chi_{1,z}, & y\gamma_{1,z} &\sim -z\zeta_{1,y},\end{aligned}\quad (29)$$

where commas stand for partial differentiation. The solution in terms of integration constants C_i is

$$\begin{aligned}t\tau_1(x, y, z, t) &= C_4x + C_5y - \sqrt{m_2/m}y + C_8z + C_9, \\ x\chi_1(x, y, z, t) &= -C_1y + C_2z + C_4t + C_3, \\ y\gamma_1(x, y, z, t) &= -C_1x + C_7z + C_5t + C_6, \\ z\zeta_1(x, y, z, t) &= -C_2x - C_7y + C_8t + C_{10}.\end{aligned}\quad (30)$$

For simplicity, we choose all $C_i = 0$ except $C_5 = \sqrt{m_2/m}$. Physically, this means that the coordinate systems have, at this order, the same origin and are not rotated or boosted with respect to each other. These constants represent the 10 degrees of freedom of the Poincaré group.

The coordinate transformation then becomes

$$\begin{aligned}\bar{X} &\approx \left(x - \frac{m_2b}{m}\right) + x\left[\left(\frac{m_2}{b}\right)\chi_2(x^\mu) + \left(\frac{m_2}{b}\right)^{3/2}\chi_3(x^\mu)\right], \\ \bar{Y} &\approx y\left[1 + \left(\frac{m_2}{b}\right)\gamma_2(x^\mu) + \left(\frac{m_2}{b}\right)^{3/2}\gamma_3(x^\mu)\right], \\ \bar{Z} &\approx z\left[1 + \left(\frac{m_2}{b}\right)\zeta_2(x^\mu) + \left(\frac{m_2}{b}\right)^{3/2}\zeta_3(x^\mu)\right], \\ \bar{T} &\approx t\left[1 + \left(\frac{m_2}{b}\right)\tau_2(x^\mu) + \left(\frac{m_2}{b}\right)^{3/2}\tau_3(x^\mu)\right],\end{aligned}\quad (31)$$

where the errors are still $O(2, 3)$.

Applying asymptotic matching to $O(m/b)$, we obtain

$$\begin{aligned}-(\tau_2 + t\tau_{2,t}) &\sim 1 - \frac{(x - m_2b/m)}{b} = 1 - \frac{x_1}{b}, \\ \chi_2 + x\chi_{2,x} &\sim 1 - \frac{(x - m_2b/m)}{b} = 1 - \frac{x_1}{b}, \\ \gamma_2 + y\gamma_{2,y} &\sim 1 - \frac{(x - m_2b/m)}{b} = 1 - \frac{x_1}{b}, \\ \zeta_2 + z\zeta_{2,z} &\sim 1 - \frac{(x - m_2b/m)}{b} = 1 - \frac{x_1}{b}, \\ x\chi_{2,t} - t\tau_{2,x} &\sim \frac{t}{b} + \left(\frac{m}{m_2}\right)^{1/2}\frac{y}{b}\kappa_1, \\ y\gamma_{2,t} - t\tau_{2,y} &\sim -\left(\frac{m}{m_2}\right)^{1/2}\frac{x - m_2b/m}{b}\kappa_1, \\ z\zeta_{2,t} &\sim t\tau_{2,z}, \\ x\chi_{2,y} &\sim -y\gamma_{2,x}, \\ x\chi_{2,z} &\sim -z\zeta_{2,x}, \\ \gamma_{2,z} &\sim -z\zeta_{2,y}.\end{aligned}\quad (32)$$

Once more we have a system of 10 coupled partial differential equations. We can choose any κ_1 , thus determining the (m/b) part of the coordinate transformation. For simplicity, we choose $\kappa_1 = 0$, which implies that the coordinate systems are not rotating with respect to each other. The solution to this system is then given by

$$\begin{aligned}\tau_2 &= -\left[1 - \frac{x}{b} + \frac{x^2}{b^2} - \left(\frac{m_2}{m} - \frac{x}{b}\right)^2\right] + D_5\frac{y}{t} + D_4\frac{x}{t} + D_8\frac{z}{t} + \frac{D_9}{t}, \\ \chi_2 &= 1 - \frac{x}{2b} + \frac{x^2}{4b^2} - \left(\frac{m_2}{m} - \frac{x}{2b}\right)^2 + \frac{1}{xb}\left(t^2 + \frac{y^2 + z^2}{2}\right) - \frac{m_2}{mxb}(t^2 + y^2 + z^2) + D_1\frac{y}{x} + D_4\frac{t}{x} + D_2\frac{z}{x} + \frac{D_3}{x}, \\ \gamma_2 &= 1 - \frac{x}{b} + \frac{x^2}{b^2} - \left(\frac{m_2}{m} - \frac{x}{b}\right)^2 - D_1\frac{x}{y} + D_7\frac{z}{y} + D_5\frac{t}{y} + \frac{D_6}{y}, \\ \zeta_2 &= 1 - \frac{x}{b} + \frac{x^2}{b^2} - \left(\frac{m_2}{m} - \frac{x}{b}\right)^2 + D_8\frac{t}{z} - D_7\frac{y}{z} - D_2\frac{x}{z} + \frac{D_{10}}{z},\end{aligned}\quad (33)$$

where the D_i are more undetermined coefficients. Once more, using the 10 degrees of freedom of the Poincaré group,

we set all coefficients to zero, and the coordinate transformation becomes

$$\begin{aligned}\bar{X} &\approx \left(x - \frac{m_2 b}{m}\right) + x \left\{ \left(\frac{m_2}{b}\right) \left[1 - \frac{(x - 2m_2 b/m)}{2b}\right] + \left(\frac{m_2}{b}\right)^{3/2} \chi_3(x^\mu) \right\} + \frac{m_2}{2b^2} (2t^2 + y^2 + z^2), \\ \bar{Y} &\approx y \left\{ 1 + \left(\frac{m_2}{b}\right) \left[1 - \frac{(x - m_2 b)/m}{b}\right] + \left(\frac{m_2}{b}\right)^{3/2} \gamma_3(x^\mu) \right\} + \omega \frac{m_2 b}{m} t, \\ \bar{Z} &\approx z \left\{ 1 + \left(\frac{m_2}{b}\right) \left[1 - \frac{(x - m_2 b)/m}{b}\right] + \left(\frac{m_2}{b}\right)^{3/2} \zeta_3(x^\mu) \right\}, \\ \bar{T} &\approx t \left\{ 1 - \left(\frac{m_2}{b}\right) \left[1 - \frac{(x - m_2 b/m)}{b}\right] + \left(\frac{m_2}{b}\right)^{3/2} \tau_3(x^\mu) \right\},\end{aligned}\quad (34)$$

with errors of $O(2, 3)$.

Now that matching has been completed to $O(m/b)^0$, $O(m/b)^{1/2}$ and $O(m/b)$, we can proceed with matching at $O(m/b)^{3/2}$. However, keeping in mind our discussion in Sec. III of the order needed, we will only use the spatial-temporal part of the asymptotic relations matrix (28),

$$\begin{aligned}x\chi_{3,t} - t\tau_{3,x} &\sim \left(\frac{m}{m_2}\right)^{1/2} \left[\frac{y}{b} \left(1 - \kappa_2 - \frac{4x}{b} + 3\frac{m_2}{m}\right) \right], \\ t\tau_{3,y} - y\gamma_{3,t} &\sim \left(\frac{m}{m_2}\right)^{1/2} \left(\frac{x}{b} \left[\kappa_2 - 1 + \frac{4m_1 - 6m_2}{m} - 4\left(\frac{m_2}{m}\right)^2 + 8\frac{\mu}{m} \right] + \left(\frac{x}{b}\right)^2 \left(\frac{11}{2} + \frac{2m_1}{m} \right) \right. \\ &\quad \left. + \left(\frac{y}{b}\right)^2 \left(\frac{3}{2} - \frac{3m_2}{m} \right) + \left(\frac{z}{b}\right)^2 \left(\frac{1}{2} - \frac{3m_2}{m} \right) + \left(\frac{t}{b}\right)^2 + \frac{4\mu b}{m_2 r_1} \right. \\ &\quad \left. + \left\{ \frac{m_2}{m} \left[1 - \kappa_2 + 2\left(\frac{m_2}{m}\right)^2 + \frac{3m_2 - 4\mu}{m} \right] - 4\frac{\mu + m_1}{m} \right\} \right), \\ t\tau_{3,z} - z\zeta_{3,t} &\sim \left(\frac{m}{m_2}\right)^{1/2} \frac{zy}{b^2}.\end{aligned}\quad (35)$$

From asymptotic analysis, we know that κ_2 must be coordinate independent, but from Eqs. (35) it is clear that we have an arbitrary infinite number of choices, all of which will lead to a different coordinate transformation. For simplicity, we choose $\kappa_2 = 1 + 3m_2/m$. This completes the derivation of the matching parameters, since η_i and κ_3 did not appear in the differential equations at all, and hence, we can neglect them to this order. Note that this choice of parameter matching is different from Alvi's

choice, so our coordinate transformation is also different. Up to $O(m/b)^2$, we then obtain the following matching condition ψ_{13} :

$$\Omega \approx \omega \left[1 + \frac{m_2}{b} \left(1 + 3\frac{m_2}{m} \right) \right], \quad M_1 \approx m_1. \quad (36)$$

This choice of ψ_{13} simplifies Eq. (35), which now becomes

$$\begin{aligned}t\tau_{3,x} - x\chi_{3,t} &\sim - \left(\frac{m}{m_2}\right)^{1/2} \frac{4yx}{b^2}, \\ t\tau_{3,z} - z\zeta_{3,t} &\sim \left(\frac{m}{m_2}\right)^{1/2} \frac{zy}{b^2}, \\ t\tau_{3,y} - y\gamma_{3,t} &\sim \left(\frac{m}{m_2}\right)^{1/2} \left(\frac{x}{b} \left[\frac{4m_1 - 6m_2}{m} - 4\left(\frac{m_2}{m}\right)^2 + 8\frac{\mu}{m} \right] + \left(\frac{x}{b}\right)^2 \left(\frac{11}{2} + \frac{2m_1}{m} \right) + \left(\frac{y}{b}\right)^2 \left(\frac{3}{2} - \frac{3m_2}{m} \right) \right. \\ &\quad \left. + \left(\frac{z}{b}\right)^2 \left(\frac{1}{2} - \frac{3m_2}{m} \right) + \left(\frac{t}{b}\right)^2 + \frac{4\mu b}{m_2 r_1} + \left\{ \frac{m_2}{m} \left[2\left(\frac{m_2}{m}\right)^2 - 4\frac{\mu}{m} \right] - 4\frac{\mu + m_1}{m} \right\} \right).\end{aligned}\quad (37)$$

Any choice of $(\chi_3, \gamma_3, \zeta_3, \tau_3)$ that satisfies the above equations will produce matching for the choice of matching parameters made. In the same manner as before, we will use our Poincaré degrees of freedom to keep the initial

slices as close as possible in both coordinates systems, which implies that τ_3 cannot be inversely proportional to t . With these assumptions, it is straightforward to solve Eq. (35) and find the following particular solution:

$$\begin{aligned}\tau_3(x, y, z, t) &= 0, \\ \chi_3(x, y, z, t) &= \left(\frac{m}{m_2}\right)^{1/2} \frac{4yt}{b^2}, \\ \zeta_3(x, y, z, t) &= -\left(\frac{m}{m_2}\right)^{1/2} \frac{yt}{b^2}, \\ \gamma_3(x, y, z, t) &= -\left(\frac{m}{m_2}\right)^{1/2} \frac{t}{y} \left(\frac{x}{b} \left[\frac{4m_1 - 6m_2}{m} - 4 \left(\frac{m_2}{m}\right)^2 + 8 \frac{\mu}{m} \right] + \left(\frac{x}{b}\right)^2 \left(\frac{11}{2} + \frac{2m_1}{m} \right) + \left(\frac{y}{b}\right)^2 \left(\frac{3}{2} - \frac{3m_2}{m} \right) \right. \\ &\quad \left. + \left(\frac{z}{b}\right)^2 \left(\frac{1}{2} - \frac{3m_2}{m} \right) + \frac{1}{3} \left(\frac{t}{b}\right)^2 + \frac{4\mu b}{m_2 r_1} + \left\{ \frac{m_2}{m} \left[2 \left(\frac{m_2}{m}\right)^2 - 4 \frac{\mu}{m} \right] - 4 \frac{\mu + m_1}{m} \right\} \right). \end{aligned} \quad (38)$$

To summarize, we have found a coordinate transformation ϕ_{13} and a set of matching parameters ψ_{13} that produce asymptotic matching to $O(3/2, 3)$ in the 00 and ij components of the metric and to $O(2, 3)$ in the $0i$ components.

Note however that the γ_3 piece of the coordinate transformation becomes singular at $r_1 = 0$. To get rid of this singularity we will replace r_1 by

$$\tilde{r}_1 = \sqrt{r_1^2 + 6m^2}. \quad (39)$$

This change amounts to adding a higher order term to the coordinate transformation which has no effect in the buffer zone at the current level of accuracy, but it has the advantage that the resulting coordinate transformation is now regular at $r_1 = 0$. With this replacement the coordinate transformation is given by

$$\begin{aligned}\bar{X} &\approx \left(x - \frac{m_2 b}{m} \right) + x \left\{ \left(\frac{m_2}{b}\right) \left[1 - \frac{(x - 2m_2 b/m)}{2b} \right] + m_2 \omega \frac{4yt}{b^2} \right\} + \frac{m_2}{2b^2} (2t^2 + y^2 + z^2), \\ \bar{Y} &\approx y \left\{ 1 + \left(\frac{m_2}{b}\right) \left[1 - \frac{x - m_2 b/m}{b} \right] \right\} - m_2 \omega t \left\{ \frac{x}{b} \left[\frac{4m_1 - 6m_2}{m} - 4 \left(\frac{m_2}{m}\right)^2 + 8 \frac{\mu}{m} \right] + \left(\frac{x}{b}\right)^2 \left(\frac{11}{2} + \frac{2m_1}{m} \right) \right. \\ &\quad \left. + \left(\frac{y}{b}\right)^2 \left(\frac{3}{2} - \frac{3m_2}{m} \right) + \left(\frac{z}{b}\right)^2 \left(\frac{1}{2} - \frac{3m_2}{m} \right) + \frac{1}{3} \left(\frac{t}{b}\right)^2 + \frac{4\mu b}{m_2 \tilde{r}_1} + \frac{m_2}{m} \left[2 \left(\frac{m_2}{m}\right)^2 - 4 \frac{\mu}{m} \right] - 4 \frac{\mu + m_1}{m} \right\} \\ &\quad + \omega \frac{m_2 b}{m} t, \\ \bar{Z} &\approx z \left\{ 1 + \left(\frac{m_2}{b}\right) \left[1 - \frac{x - m_2 b/m}{b} \right] - m_2 \omega \frac{yt}{b^2} \right\}, \\ \bar{T} &\approx t \left\{ 1 - \left(\frac{m_2}{b}\right) \left[1 - \frac{x - m_2 b/m}{b} \right] \right\}, \\ \Omega &\approx \omega \left[1 + \frac{m_2}{b} \left(1 + 3 \frac{m_2}{m} \right) \right], \\ M_1 &\approx m_1. \end{aligned} \quad (40)$$

The coordinate transformation for matching in the other overlap region \mathcal{O}_{23} is obtained by the following symmetry transformation: substitute $1 \leftrightarrow 2$ and

$$x \rightarrow -x, \quad y \rightarrow -y, \quad z \rightarrow z. \quad (41)$$

In Eq. (40), t should be considered small just as x ,

y , and z are. Recall that fundamentally the overlap regions are 4-volumes, although by choosing a time slicing we have dealt with their projections on a spatial hypersurface ($m_a \ll r_a \ll b$). Just as the overlap regions span a limited range of r_A , so they span a limited range of t . The post-Newtonian metric and the

perturbed Schwarzschild metric are formally stationary, but the true physical system includes gravitational waves (not modeled here) which for example change the orbital frequency on a radiation reaction timescale. While this timescale is longer than an orbital period, which must be of order b , rotation and boosts mix space and time terms and to be safe we must keep $t \ll b$. Therefore we choose the $t = 0 = T$ slice when discussing the approximate metric in the next section, which restricts our overlap region to the intersection of this 3-surface with the overlap 4-volume.

VII. AN APPROXIMATE METRIC FOR BINARY BLACK HOLES

In this section we transform the inner zone metric in isotropic corotating coordinates to harmonic corotating coordinates, via the transformation found in the previous section. The metric in the inner zone of black hole 1 is given by

$$\begin{aligned}
g_{00}^{(1)} &\approx 2h_{01}^{(1)}J_0^xJ_0^t + 2h_{02}^{(1)}J_0^yJ_0^t + 2h_{03}^{(1)}J_0^zJ_0^t + h_{11}^{(1)}(J_0^x)^2 + h_{22}^{(1)}(J_0^y)^2 + h_{33}^{(1)}(J_0^z)^2 + h_{00}^{(1)}(J_0^t)^2 + 2h_{12}^{(1)}J_0^xJ_0^y \\
&\quad + 2h_{23}^{(1)}J_0^yJ_0^z + 2h_{13}^{(1)}J_0^xJ_0^z, \\
g_{01}^{(1)} &\approx h_{22}^{(1)}J_0^yJ_1^y + h_{11}^{(1)}J_0^xJ_1^x + h_{03}^{(1)}(J_0^zJ_1^t + J_0^tJ_1^z) + h_{01}^{(1)}(J_1^xJ_0^t + J_0^xJ_1^t) + h_{02}^{(1)}(J_0^yJ_1^t + J_1^yJ_0^t) \\
&\quad + h_{13}^{(1)}(J_1^xJ_0^z + J_0^xJ_1^z) + h_{23}^{(1)}(J_1^yJ_0^z + J_0^yJ_1^z) + h_{12}^{(1)}(J_1^xJ_0^y + J_0^xJ_1^y) + h_{00}^{(1)}J_0^tJ_1^t + h_{33}^{(1)}J_0^zJ_1^z, \\
g_{02}^{(1)} &\approx h_{13}^{(1)}(J_2^xJ_0^z + J_0^xJ_2^z) + h_{23}^{(1)}(J_2^yJ_0^z + J_0^yJ_2^z) + h_{12}^{(1)}(J_2^xJ_0^y + J_0^xJ_2^y) + h_{33}^{(1)}J_0^zJ_2^z + h_{22}^{(1)}J_0^yJ_2^y \\
&\quad + h_{11}^{(1)}J_0^xJ_2^x + h_{03}^{(1)}J_0^tJ_2^z + h_{02}^{(1)}J_0^tJ_2^y + h_{01}^{(1)}J_0^tJ_2^x, \\
g_{03}^{(1)} &\approx h_{13}^{(1)}(J_3^xJ_0^z + J_0^xJ_3^z) + h_{23}^{(1)}(J_3^yJ_0^z + J_0^yJ_3^z) + h_{12}^{(1)}(J_3^xJ_0^y + J_0^xJ_3^y) + h_{33}^{(1)}J_0^zJ_3^z + h_{22}^{(1)}J_0^yJ_3^y \\
&\quad + h_{11}^{(1)}J_0^xJ_3^x + h_{03}^{(1)}J_0^tJ_3^z + h_{02}^{(1)}J_0^tJ_3^y + h_{01}^{(1)}J_0^tJ_3^x, \\
g_{11}^{(1)} &\approx 2h_{01}^{(1)}J_1^xJ_1^t + 2h_{02}^{(1)}J_1^yJ_1^t + 2h_{03}^{(1)}J_1^zJ_1^t + h_{11}^{(1)}(J_1^x)^2 + h_{22}^{(1)}(J_1^y)^2 + h_{33}^{(1)}(J_1^z)^2 + h_{00}^{(1)}(J_1^t)^2 + 2h_{12}^{(1)}J_1^xJ_1^y \\
&\quad + 2h_{23}^{(1)}J_1^yJ_1^z + 2h_{13}^{(1)}J_1^xJ_1^z, \\
g_{22}^{(1)} &\approx h_{11}^{(1)}(J_2^x)^2 + h_{22}^{(1)}(J_2^y)^2 + h_{33}^{(1)}(J_2^z)^2 + 2h_{12}^{(1)}J_2^xJ_2^y + 2h_{23}^{(1)}J_2^yJ_2^z + 2h_{13}^{(1)}J_2^xJ_2^z, \\
g_{33}^{(1)} &\approx h_{11}^{(1)}(J_3^x)^2 + h_{22}^{(1)}(J_3^y)^2 + h_{33}^{(1)}(J_3^z)^2 + 2h_{12}^{(1)}J_3^xJ_3^y + 2h_{23}^{(1)}J_3^yJ_3^z + 2h_{13}^{(1)}J_3^xJ_3^z, \\
g_{12}^{(1)} &\approx h_{13}^{(1)}(J_2^xJ_1^z + J_1^xJ_2^z) + h_{23}^{(1)}(J_2^yJ_1^z + J_1^yJ_2^z) + h_{12}^{(1)}(J_2^xJ_1^y + J_1^xJ_2^y) + h_{33}^{(1)}J_1^zJ_2^z + h_{22}^{(1)}J_1^yJ_2^y \\
&\quad + h_{11}^{(1)}J_1^xJ_2^x + h_{03}^{(1)}J_1^tJ_2^z + h_{02}^{(1)}J_1^tJ_2^y + h_{01}^{(1)}J_1^tJ_2^x, \\
g_{13}^{(1)} &\approx h_{13}^{(1)}(J_3^xJ_1^z + J_1^xJ_3^z) + h_{23}^{(1)}(J_3^yJ_1^z + J_1^yJ_3^z) + h_{12}^{(1)}(J_3^xJ_1^y + J_1^xJ_3^y) + h_{33}^{(1)}J_1^zJ_3^z + h_{22}^{(1)}J_1^yJ_3^y \\
&\quad + h_{11}^{(1)}J_1^xJ_3^x + h_{03}^{(1)}J_1^tJ_3^z + h_{02}^{(1)}J_1^tJ_3^y + h_{01}^{(1)}J_1^tJ_3^x, \\
g_{23}^{(1)} &\approx h_{11}J_2^xJ_3^x + h_{22}^{(1)}J_2^yJ_3^y + h_{33}^{(1)}J_2^zJ_3^z + h_{12}^{(1)}(J_2^xJ_3^y + J_3^xJ_2^y) + h_{23}^{(1)}(J_2^yJ_3^z + J_3^yJ_2^z) \\
&\quad + h_{13}^{(1)}(J_2^xJ_3^z + J_3^xJ_2^z), \tag{42}
\end{aligned}$$

where in the buffer zone the g_{00} and g_{ij} are accurate to $O(1, 3)$ while the g_{0i} are accurate to order $O(3/2, 3)$. In the above equation we have used the non-zero components of the Jacobian $J_\nu^\mu = \partial_\nu \bar{X}^\mu$, which are expanded as

$$\begin{aligned}
J_0^t &= 1 - \frac{m_2}{b} \left(1 - \frac{x - m_2 b/m}{b} \right), \\
J_1^t &= \frac{m_2 t}{b^2}, \\
J_0^x &= \frac{m_2}{b} \left(\frac{2t}{b} + 4 \frac{xy\omega}{b} \right), \\
J_1^x &= 1 + \frac{m_2}{b} \left(1 - \frac{x - m_2 b/m}{b} + \frac{4\omega y t}{b} \right), \\
J_2^x &= \frac{m_2}{b} \left(\frac{y}{b} + 4 \frac{x\omega t}{b} \right), \\
J_3^x &= \frac{m_2 z}{b^2}, \\
J_0^y &= \frac{m_2}{m} \omega b - m_2 \omega \left\{ \frac{x}{b} \left[\frac{4m_1 - 6m_2}{m} - 4 \left(\frac{m_2}{m} \right)^2 + 8 \frac{\mu}{m} \right] + \left(\frac{x}{b} \right)^2 \left(\frac{11}{2} + \frac{2m_1}{m} \right) + \left(\frac{y}{b} \right)^2 \left(\frac{3}{2} - \frac{3m_2}{m} \right) \right. \\
&\quad \left. \left(\frac{z}{b} \right)^2 \left(\frac{1}{2} - \frac{3m_2}{m} \right) + \left(\frac{t}{b} \right)^2 + \frac{4\mu b}{m_2 \tilde{r}_1} + \frac{m_2}{m} \left[2 \left(\frac{m_2}{m} \right)^2 - 4 \frac{\mu}{m} \right] - 4 \frac{\mu + m_1}{m} \right\}, \\
J_1^y &= \frac{-m_2}{b} \frac{y}{b} - m_2 \omega t \left\{ \frac{1}{b} \left[\frac{4m_1 - 6m_2}{m} - 4 \left(\frac{m_2}{m} \right)^2 + 8 \frac{\mu}{m} \right] + \frac{2x}{b^2} \left(\frac{11}{2} + \frac{2m_1}{m} \right) - 4 \frac{\mu b}{m_2} \frac{x - m_2 b/m}{\tilde{r}_1^3} \right\}, \\
J_2^y &= 1 + \frac{m_2}{b} \left(1 - \frac{x - m_2 b/m}{b} \right) - m_2 \omega t \left[\frac{2y}{b^2} \left(\frac{3}{2} - \frac{3m_2}{m} \right) - 4 \frac{\mu b}{m_2} \frac{y}{\tilde{r}_1^3} \right], \\
J_3^y &= -m_2 \omega t \left[\frac{2z}{b^2} \left(\frac{1}{2} - \frac{3m_2}{m} \right) - 4 \frac{\mu b}{m_2} \frac{z}{\tilde{r}_1^3} \right], \\
J_0^z &= -m_2 \omega \frac{zy}{b^2}, \\
J_1^z &= -m_2 \frac{z}{b^2}, \\
J_2^z &= -m_2 \omega \frac{zt}{b^2}, \\
J_3^z &= 1 + \frac{m_2}{b} \left(1 - \frac{x - m_2 b/m}{b} \right) - m_2 \omega \frac{yt}{b^2}. \tag{43}
\end{aligned}$$

Furthermore, $h_{\mu\nu}^{(1)}$ refers to the inner metric as presented in Eq. (23), where we substitute the coordinate transformation given by Eq. (40) and

$$R_1 = (\bar{X}^2 + \bar{Y}^2 + \bar{Z}^2)^{1/2}. \tag{44}$$

The metric in the inner zone of black hole 2 (\mathcal{C}_2) is given by the symmetry transformation presented in the previous section when applied to Eq. (42). The near zone metric is given by Eq. (15).

Eq. (15), Eq. (42) and the symmetry transformed version of Eq. (42) represent a piecewise approximate solution to the Einstein equations. The inner zone pieces of this metric are accurate to $O(R_1/b)^2$, while the post-Newtonian near zone pieces are accurate to $O(m/r)^{3/2}$. In the overlap region, the inner and near zone $0i$ components match up to $O(3/2, 2)$, while all other components match only up to $O(1, 2)$. If all components were matched

only up to $O(1, 2)$ asymptotic matching would imply using Eq. (34), with $\zeta_3, \tau_3, \gamma_3$ and χ_3 set to zero, for the coordinate transformation. However, since numerical simulations also require the extrinsic curvature to $O(m/b)^{3/2}$, it was necessary to find a coordinate transformation that produces matching in the $0i$ components to higher order. The inner zone pieces of the metric presented here use the full coordinate transformation of Eq. (40) which is slightly more accurate than what we would have obtained if we had used Eq. (34).

Note that when we applied the coordinate transformation (40) to the inner zone metric we kept terms up to $O(m/b)^5$. This is because the inner zone metric represents a tidally perturbed black hole with errors in the physics of $O(1, 3)$. Close to BH1 ($R_1 \sim m$), the error in the physics is only of order $O(m/b)^4$ and hence we should keep terms to at least order $O(m/b)^3$. However, recall that the perturbed black hole metric satisfies

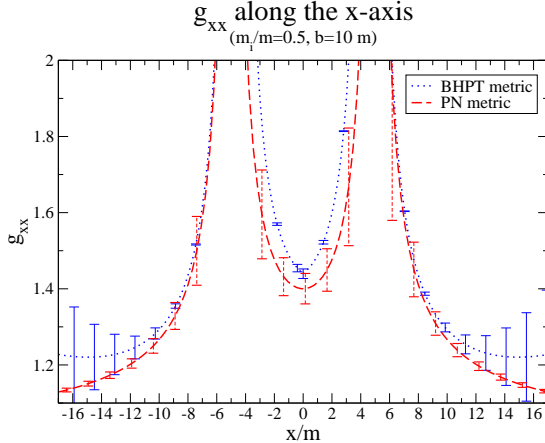


FIG. 4: This figure shows the xx component of the near zone metric (dashed line) and the inner zone metric (solid line) along the (harmonic) x axis for a perturbative parameter $m/b = 1/10$, with the black holes located at $x/m \approx \pm 5$. Observe that the metrics become asymptotic to each other near the black holes. Also plotted are estimates of the error in the approximations given by $2[(m_1/r_1)^2 + (m_2/r_2)^2]$ for the near zone metric and $2(m/b)(r/b)^3$ for the inner zone metric.

the Einstein equations up to errors of only $O(2, 4)$ even though its astrophysical resemblance to a binary black hole has errors already at $O(1, 3)$. If we want to obtain a metric which is close to the constraint hypersurface, we should keep terms larger than $O(1, 3)$, but not larger than $O(2, 4)$. In particular, close to the black hole we have constraint violation of $O(m/b)^6$. For example, if we had dropped terms of order $O(m/b)^4$ in the inner zone metric we would have introduced additional constraint violations at this order.

A. Global character of the asymptotic metric

The global character of this metric is demonstrated in Figs. 4 and 5. These figures show the xx and 00 component of the global metric along the x axis for two equal-mass black holes $m_A/m = 0.5$ located at $x/m \approx \pm 5$. We found that the buffer zone is formally $m_A \ll r_A \ll b$, so in dimensionless units the buffer zone for black hole 1 is approximately $5.5 \ll x/m \ll 15$. The curves for the two local approximate metric components are close to each other in this region, but diverge from each other as $r \rightarrow \infty$. If the perturbation parameter m/b were taken to be smaller, the curves would be even closer to each other.

The error bars presented in the figures are $E_{PN} = 2[(m_1/r_1)^2 + (m_2/r_2)^2]$ and $E_{BHPT} = 2(m/b)(r_A/b)^3$. The error in the near zone metric was determined by looking at the next order (2 PN) term in the metric components [27]. The factor of 2 in the error of the inner zone metric comes about because the next correction in

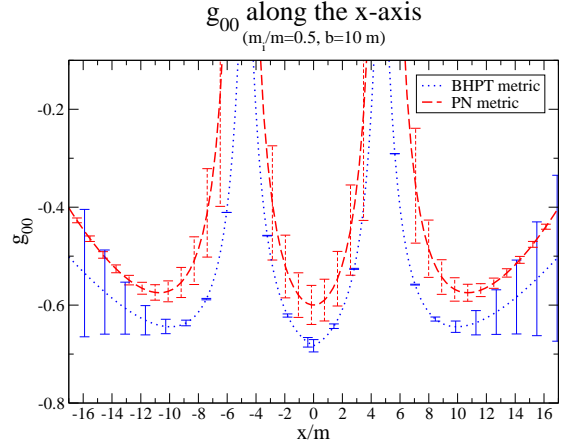


FIG. 5: This figure is identical to Fig. 4, but it shows the 00 component of the metric. Observe that in this component the differences between the different approximations are more pronounced, although the general features of asymptotic matching are clearly still discernible.

perturbation theory will be proportional to

$$E_{BHPT} \approx \frac{1}{3} R_{i0j0,k} \approx 2m/b^4 r^3. \quad (45)$$

The error bars of the respective approximations shrink or expand depending on the location of the field point, providing a useful sign of where the approximation is breaking down. Both figures show that the different approximation schemes diverge in different places. The inner zone metric is shifted slightly toward the center of mass of the system due to the coordinate transformation used in the matching. The dominant factor in this shift is roughly $m_{1,2}/2$, which corresponds to the fact that harmonic coordinates put the horizon at $r_{1,2} = m_{1,2}$, while isotropic coordinates put it at $R_{1,2} = M_{1,2}/2$.

Since both curves diverge as $r_A \rightarrow 0$, it might seem that the solutions approach each other near the horizons. This misconception can be rectified by scaling the solutions to the Brill-Lindquist factor ψ^4 , where

$$\psi = 1 + \frac{m_1}{2r_1} + \frac{m_2}{2r_2}. \quad (46)$$

This removes most of the divergent behavior of the solutions, as shown in Fig. 6. Observe that the near zone solution diverges earlier, which agrees with the previous observation that the PN location of the black hole has shifted. Furthermore, the manner in which the solutions diverge is completely different. The inner zone metric diverges always toward negative infinity, whereas the near zone solution is always positive between the black holes.

B. Transition Functions

We have constructed a global approximate solution for a binary black hole system as a piece-wise function,

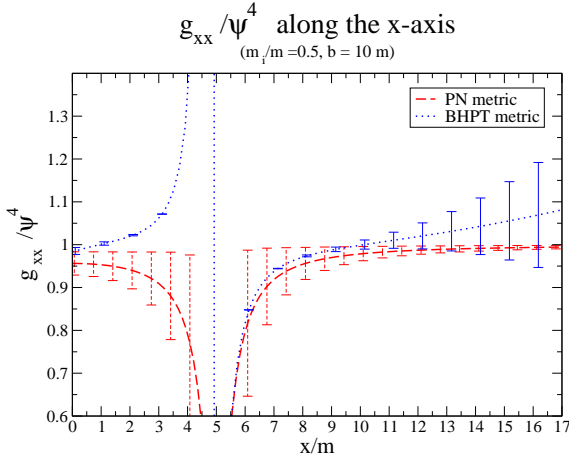


FIG. 6: In this figure we plot the xx component of the near zone (dashed line) and inner zone (solid line) metrics divided by ψ^4 . The divergent behavior of the solutions is clearly different as we approach the event horizon. The PN solution diverges toward positive infinity between the black holes. Furthermore, the BHPT solution diverges more steeply than the PN solution.

each piece of which approaches each other asymptotically in some 3-volume. The size of the discontinuities will depend slightly on the choice of matching radius. Nonetheless, these discontinuities will be at most of order $O(3/2, 3)$ as expected, which can be made smaller than numerical resolution by choosing a sufficiently small parameter m/b . However, doing so, implies pushing the black holes farther apart, which is not the region of interest for numerical relativity. We now construct transition functions that smooth these discontinuities out, by letting

$$g_{\mu\nu}^{(1,3)} = [1 - F_1(R_1)] g_{\mu\nu}^{(1)} + F_1(R_1) g_{\mu\nu}^{(3)}, \quad (47)$$

where F_1 has the asymptotic properties that $F_1(R_1 \rightarrow \infty) \rightarrow 1$, $F_1(R_1 \rightarrow 0) \rightarrow 0$, $F_1(R_1 \sim r_1^M) \sim 1/2$. This solution merges the solutions valid in \mathcal{C}_1 and \mathcal{C}_3 , and hence it is valid in $\mathcal{C}_1 \cup \mathcal{C}_3$. A similar solution can be obtained for the other black hole ($\mathcal{C}_2 \cup \mathcal{C}_3$) by replacing $1 \rightarrow 2$.

A Fermi-Dirac distribution could serve as such a transition function:

$$F_1(R_1) = \frac{1}{2} \left\{ 1 + \tanh \left[0.2 \frac{R_1}{m} \left(1 - \left(\frac{r_1^M}{R_1} \right)^2 \right) \right] \right\}. \quad (48)$$

However, since this function is nowhere zero, $g_{\mu\nu}^{(1,3)}$ in Eq. (47) will always be contaminated by a solution that is not valid in that region. For example, if we used the above transition function the global metric would necessarily blow up at the location of the point particle that represents the black hole in post-Newtonian theory. However, the PN metric is not valid in that region, and hence, this spurious divergence would contaminate the global metric.

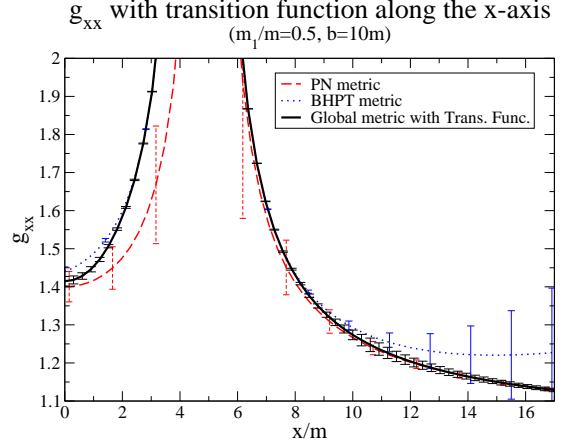


FIG. 7: In this figure we show the transition function as it takes the xx component of the near zone metric to the inner zone solution around BH 1. Observe that the transition function is smooth and does not introduce kinks into the global solution.

In order to eliminate these spurious divergences, we will use transition functions of the form

$$f(r) = \begin{cases} 0, & r \leq r_0 \\ \frac{1}{2} \left\{ 1 + \tanh \left[\frac{s}{\pi} \left(\tan \left(\frac{\pi}{2w} (r - r_0) \right) - \frac{q^2}{\tan \left(\frac{\pi}{2w} (r - r_0) \right)} \right)^2 \right] \right\}, & r_0 < r < r_0 + w \\ 1, & r \geq r_0 + w \end{cases}, \quad (49)$$

which ensures that $f(r)$ is identically zero in a whole region around $r = 0$. This function transitions from zero to one in a boundary layer of width w , by compactifying infinity into a finite region. The parameter choice for the transition function will depend on the system that is being analyzed. For the test system ($m_A/m = 0.5$ and $b = 10m$) a good choice seems to be

$$F_A(R_A) = f(R_A), \quad (50)$$

with

$$r_0 = 1.5m, \quad w = 4r_A^M, \quad q = 1/4, \quad s = b/m, \quad (51)$$

where

$$r_A^M = (b^4 m_A^2 / m)^{1/5}. \quad (52)$$

The function $F_A(R_A)$ satisfies the necessary asymptotic relations. If we take the asymptotic limit $R_A \gg r_A^M$, $F_A(R_A) = 1$ and similarly, as $R_A \ll r_A^M$, $F_A(R_A) = 0$. Observe that this choice of matching radius r_A^M agrees with our previous dimensional analysis (Eq. 11) with $\beta = m_2/m$.

We can see the effect of this transition function in Fig. 7 and 8. The transition function effectively takes one solution into the other smoothly in a region where the error bars are of the same order. The size of the boundary

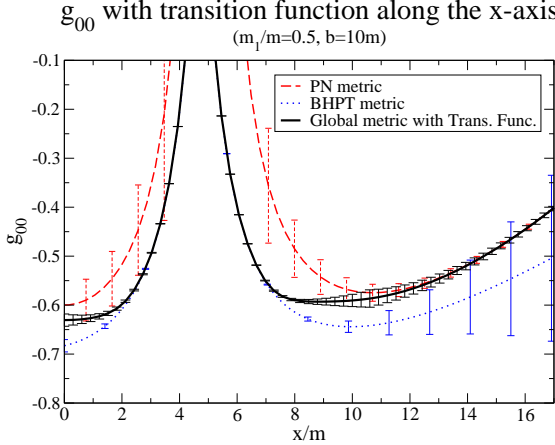


FIG. 8: In this figure we show the transition function as it takes the 00 component of the near zone metric to the inner zone solution around black hole 1.

layer can be modified by changing the “thickness” w , but if w is made too small the derivatives of the metric (which include $1/w$ terms) develop artificial peaks in the boundary layer. Hence, care must be taken when choosing these parameters by looking not only at the metric, but also at the extrinsic curvature.

Furthermore, we have to construct a third function to allow for a smooth transition between the two black holes. This function $G(x)$ will be of the same form as the function in Eq. 49, *i.e.*

$$G(x) = f(x), \quad (53)$$

but with different parameters given by

$$r_0 = \frac{b(m_2 - m_1)}{2m} - \frac{b - m}{2}, \quad w = b - m, \quad q = 1, \quad s = 5/2. \quad (54)$$

With these transition functions, we can construct a uniform approximation of the metric, valid in $\mathcal{C}_1 \cup \mathcal{C}_2 \cup \mathcal{C}_3 \cup \mathcal{C}_4$, namely

$$\begin{aligned} g_{\mu\nu}^{(global)} = & G(x) \left\{ F_1(R_1) g_{\mu\nu}^{(1)} [1 - F_1(R_1)] g_{\mu\nu}^{(3)} \right\} \\ & + [1 - G(x)] \left\{ F_2(R_2) g_{\mu\nu}^{(2)} + [1 - F_2(R_2)] g_{\mu\nu}^{(3)} \right\}, \end{aligned} \quad (55)$$

where $g_{\mu\nu}^{(1)}$ stands for the metric (42) that applies to the inner zone of black hole 1 (\mathcal{C}_1), and $g_{\mu\nu}^{(2)}$ stands for the metric valid in the inner zone of black hole 2 (\mathcal{C}_2). As shown in Figs. 9 and 10, we have removed the piecewise behavior of the solution.

We emphasize that different systems with different masses and at different separations will have different optimal transition functions, although the matched solutions should still work. Nonetheless, the transition

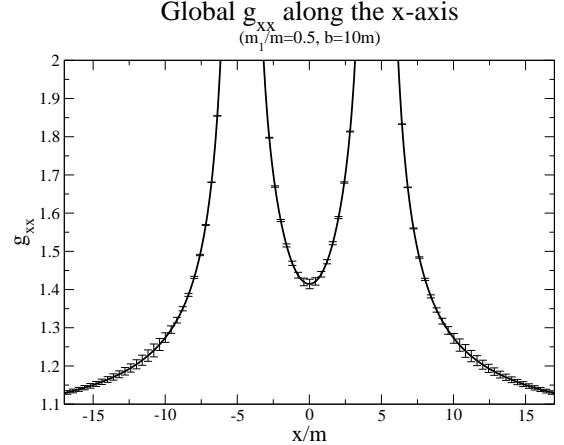


FIG. 9: This figure shows the xx component of the global approximation of the metric with the transition functions that remove the discontinuities due to the piece-wise behavior. This figure corresponds again to the same test system discussed earlier.

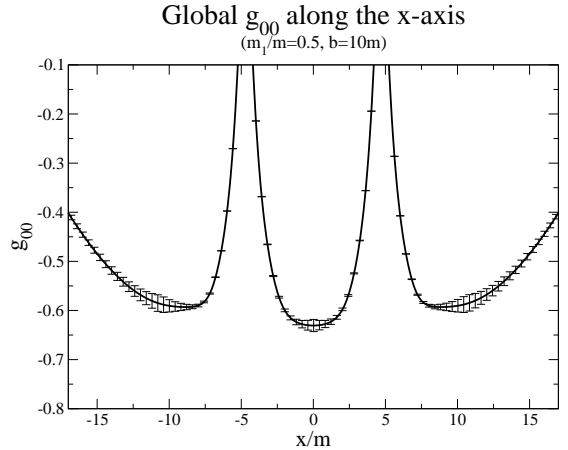


FIG. 10: This figure shows the 00 component of the global metric along the x -axis. The same test system has been used as before.

functions constructed here are general enough that they should in principle work for most masses at most separations with the appropriate choice of parameters. Note that when constructing transition functions for other astrophysical systems care must also be taken to not change much the differentiability properties of the original $g_{\mu\nu}^{(1)}$, $g_{\mu\nu}^{(2)}$ and $g_{\mu\nu}^{(3)}$, so that no spurious discontinuities are introduced in the extrinsic curvature.

Our approximate metric should not be used for binaries with separations so small that the inner zones of the two black holes are no longer separated by part of the near zone—*i.e.*, that the buffer zone disappears. Since the precise radii of convergence of the PN and BHPT series are not known, we cannot know the minimum separation

precisely. However, our numerical explorations indicate that it is always less than $10m$ and goes down to about $7m$ in the case where the black holes have equal masses.

Numerical evolutions using our initial data will need to excise the black holes. The excision region can in principle be just inside the horizon (or the causally disconnected region), but it helps to bring it in a little bit. How far can that be done? The tidal perturbation used to obtain the inner zone metric is valid only for small spacelike separations from the event horizon, and thus the isotropic coordinate R_A must be greater than some minimum value. For a single perturbed black hole, this value is the one corresponding to the same value of harmonic r_A in the causally disconnected region. If the maximum value of r_A for which the perturbation is valid is roughly $(m_A/m)b$, and if $b \gg m$ as it must be for our initial data to be valid, then the maximum R_A is roughly $(m_A/m)b$ as well. In the causally disconnected region of the Schwarzschild spacetime, the R_A corresponding to the same value of r_A on that patch is given by the transformation $R_A \rightarrow (m_1/2)^2/R_A$ (where we have used $m_1 \approx M_1$). Thus the tidal perturbation is good roughly for

$$\frac{m_A m}{2b} \ll R_A \ll \frac{m_A}{m} b. \quad (56)$$

The excision radius in harmonic coordinates can be chosen anywhere between the lower limit of this expression and the upper limit $m_A/2$ at the horizon.

VIII. INITIAL DATA FOR NUMERICAL RELATIVITY

The approximate metric (55) could be used as initial data for binary black hole simulations. To facilitate this task we now present this metric in the $3 + 1$ decomposition, by providing explicit analytic expressions for the extrinsic curvature, lapse and shift on the $\bar{T} = t = 0$ slice. If the normal vector to this slice is denoted by n^a , then the intrinsic metric in the slice is given by

$$q_{ab} = g_{ab} + n_a n_b, \quad (57)$$

and the extrinsic curvature is

$$K_{ab} = -\frac{1}{2} \mathcal{L}_n q_{ab}, \quad (58)$$

where \mathcal{L}_n is the Lie derivative in the direction normal to the $t = 0$ -slice. Below we compute K_{ab} using the explicit

expression

$$K_{ab} = -\frac{1}{2} n^c (\partial_c q_{ab} - \partial_a q_{cb} - \partial_b q_{ac}), \quad (59)$$

which has been obtained using the ordinary derivative operator and the fact that $q_{ab} n^b = 0$. The evolution vector

$$(\partial_t)^a = \alpha n^a + \beta^a \quad (60)$$

is split into pieces perpendicular and parallel to the $t = 0$ slice, where α denotes the lapse and β^a the shift. Note that $n^a n_a = -1$ and $\beta^a n_a = 0$.

The near zone extrinsic curvature computed from the PN metric [27] in corotating harmonic coordinates on the $t = 0$ slice is given by

$$K_{ij}^{(3)} = \sum_{A=1}^2 m_A \frac{4v_A^{(i)} n_A^{(j)} - v_A^k n_k^A \delta_{ij}}{r_A^2}, \quad (61)$$

where the superscript 3 is to remind us that this expression is only valid in \mathcal{C}_3 , and where the parenthesis on the indices stands for symmetrization. In the previous equation, v_A^i and n_A^i denotes the particle velocities and directional vectors given by

$$v_1^2 = \omega \frac{m_2}{m} b, \quad v_2^2 = -\omega \frac{m_1}{m} b, \quad v_A^1 = v_A^3 = 0 \quad (62)$$

and

$$n_A^k = \frac{x^k - x_A^k}{r_A}, \quad x_1^1 = \frac{m_2}{m} b, \quad x_2^1 = -\frac{m_1}{m} b, \quad x_A^2 = x_A^3 = 0. \quad (63)$$

The corresponding near zone lapse and shift on the $t = 0$ slice are

$$\alpha_{(3)} = 1 - \sum_{A=1}^2 \frac{m_A}{r_A} \quad (64)$$

and

$$\beta_{(3)}^i = - \sum_{A=1}^2 \frac{4m_A v_A^i}{r_A} - \epsilon_{ij3} \omega x^j, \quad (65)$$

where once more this is valid on \mathcal{C}_3 .

The extrinsic curvature of the $\bar{T} = 0$ slice valid in the inner zone of black hole 1 (\mathcal{C}_1) and computed from the metric given in the previous section in isotropic corotating coordinates is

$$\begin{aligned}
K_{00}^{(1),ICC} &= -\frac{m_2}{b^3}\Omega^2\bar{Y}(\bar{X}^2 + \bar{Y}^2)\frac{\Psi^5}{\Psi - \frac{M_1}{R_1}}\left[2\left(\Psi - \frac{M_1}{R_1}\right)^2b\omega + 3\Omega\bar{X}\left(\Psi^4 - \frac{2M_1^2}{R_1^2}\right)\right], \\
K_{01}^{(1),ICC} &= \frac{m_2}{b}\Omega\frac{\Psi^5}{\Psi - \frac{M_1}{R_1}}\left[3\Omega\bar{X}\frac{\bar{Y}^2}{b^2}\left(\Psi^4 - \frac{2M_1^2}{R_1^2}\right) + \left(\Psi - \frac{M_1}{R_1}\right)^2\frac{\omega}{b}(\bar{X}^2 + 2\bar{Y}^2) + \left(\Psi - \frac{M_1}{R_1}\right)M_1\omega\frac{\bar{X}^2}{R^3b}\right. \\
&\quad \left.(\bar{X}^2 + \bar{Y}^2 - \bar{Z}^2)\right], \\
K_{02}^{(1),ICC} &= -\frac{m_2\bar{X}\bar{Y}}{b^3}\Omega\frac{\Psi^5}{\Psi - \frac{M_1}{R_1}}\left[\left(\Psi - \frac{M_1}{R_1}\right)^2b\omega + 3\Omega\bar{X}\left(\Psi^4 - \frac{2M_1^2}{R_1^2}\right) - \left(\Psi - \frac{M_1}{R_1}\right)\frac{bM_1}{R_1^3}\omega(\bar{X}^2 + \bar{Y}^2 - \bar{Z}^2)\right], \\
K_{03}^{(1),ICC} &= \frac{m_2}{b^2}\omega\Omega\bar{X}\bar{Z}\Psi^5\left[\frac{M_1}{R_1^3}(\bar{X}^2 + \bar{Y}^2 - \bar{Z}^2) - \Psi + \frac{M_1}{R_1}\right], \\
K_{11}^{(1),ICC} &= -\frac{m_2\bar{Y}}{2b^3}\frac{\Psi^5}{\Psi - \frac{M_1}{R_1}}\left[4\left(\Psi - \frac{M_1}{R_1}\right)^2b\omega + 4\left(\Psi - \frac{M_1}{R_1}\right)b\frac{M_1}{R_1^3}\omega\bar{X}^2 - 3\Omega\bar{X}\left(4\frac{M_1^2}{R_1^2} - 2\Psi^4 + \frac{M_1^3\bar{X}^2}{R_1^5}\right.\right. \\
&\quad \left.\left. + \frac{4M_1\bar{X}^2}{R_1^3}\right)\right], \\
K_{12}^{(1),ICC} &= \frac{m_2\bar{X}}{2b^3}\frac{\Psi^5}{\Psi - \frac{M_1}{R_1}}\left[2\left(\Psi - \frac{M_1}{R_1}\right)^2b\omega + 12M_1\Omega\frac{\bar{X}\bar{Y}^2}{R_1^3}\left(1 + \frac{M_1^2}{(\Psi - \frac{M_1}{R_1})R_1^2}\right) + 2\left(\Psi - \frac{M_1}{R_1}\right)b\omega\frac{M_1}{R_1^3}\right. \\
&\quad \left.(\bar{X}^2 - \bar{Y}^2 - \bar{Z}^2)\right], \\
K_{13}^{(1),ICC} &= \frac{6M_1m_2\Omega\bar{X}^2\bar{Y}\bar{Z}}{b^3R_1^3}\frac{\Psi^5}{\Psi - \frac{M_1}{R_1}}\left(1 + \frac{M_1^2}{4R_1^2}\right), \\
K_{22}^{(1),ICC} &= \frac{m_2\bar{Y}}{2b^3}\frac{\Psi^5}{\Psi - \frac{M_1}{R_1}}\left\{12\frac{M_1^2}{R_1^2}\Omega\bar{X} - 6\Omega\Psi^4\bar{X} + 3\frac{M_1^3\bar{Y}^2}{R_1^5}\Omega\bar{X} + 4\frac{M_1}{R_1^3}\left[3\Omega\bar{X}\bar{Y}^2 + \left(\Psi - \frac{M_1}{R_1}\right)b\omega(\bar{X}^2 - \bar{Z}^2)\right]\right\}, \\
K_{23}^{(1),ICC} &= -\frac{m_2\bar{Z}}{2b^3}\frac{\Psi^5}{\Psi - \frac{M_1}{R_1}}\left[2\left(\Psi - \frac{M_1}{R_1}\right)^2b\omega - 12M_1\Omega\frac{\bar{X}\bar{Y}^2}{R_1^3}\left(1 + \frac{M_1^2}{4R_1^2}\right) - 2\left(\Psi - \frac{M_1}{R_1}\right)\frac{bM_1\omega}{R_1^3}(\bar{X}^2 + \bar{Y}^2 - \bar{Z}^2)\right], \\
K_{33}^{(1),ICC} &= \frac{m_2\bar{Y}}{2b^3}\frac{\Psi^5}{\Psi - \frac{M_1}{R_1}}\left[4\left(\Psi - \frac{M_1}{R_1}\right)^2b\omega + 4\left(\Psi - \frac{M_1}{R_1}\right)b\omega\frac{M_1\bar{Z}^2}{R_1^3} + 3\Omega\bar{X}\left(4\frac{M_1^2}{R_1^2} - 2\Psi^4 + \frac{M_1^3\bar{Z}^2}{R_1^5} + 4\frac{M_1\bar{Z}^2}{R_1^3}\right)\right], \\
\end{aligned} \tag{66}$$

where the superscript ICC is to remind that this is calculated in isotropic corotating coordinates. Later on, we will transform this metric to harmonic corotating coordinates with the map ϕ_{13} found in Eq. 40, and we will drop this superscript.

In the above equations, Ψ is the Brill-Lindquist factor for black hole 1 in isotropic coordinates, *i.e.*

$$\Psi = 1 + \frac{M_1}{2R_1}. \tag{67}$$

The $K_{0\mu}^{(1),ICC}$ components will be needed later in the

coordinate transformation and are obtained from the purely spatial components $K_{kl}^{(1),ICC}$ using

$$K_{0\nu}^{(1),ICC} = q_0^k q_\nu^l K_{kl}^{(1),ICC}, \tag{68}$$

where the projection tensor q_μ^ν is given by

$$q_\mu^\nu = \delta_\mu^\nu + n_\mu^{(1),ICC} n_{(1),ICC}^\nu. \tag{69}$$

Here, the normal vector to the slice computed with $n_a^{(1),ICC} = -\sqrt{\frac{-1}{h_{(1)}^{00}}}(dT)_a$ is given by

$$n_0^{(1),ICC} = -\frac{1 - \frac{M_1}{2R_1}}{\Psi}\left[1 - \frac{m_2}{b}\left(1 - \frac{M_1}{2R_1}\right)^2\Psi^2\frac{R_1^2}{b^2}P_2\left(\frac{\bar{X}}{R_1}\right)\right], \quad n_i^{(1),ICC} = 0, \tag{70}$$

where P_2 stands for the second Legendre polynomial.

The upper components are then

$$\begin{aligned}
n_{(1),ICC}^0 &= \frac{\Psi}{1 - \frac{M_1}{2R_1}} \left[1 + \frac{m_2}{b} \left(1 - \frac{M_1}{2R_1} \right)^2 \Psi^2 \frac{R_1^2}{b^2} P_2(\bar{X}/R_1) \right], \\
n_{(1),ICC}^1 &= \frac{\Psi}{1 - \frac{M_1}{2R_1}} \bar{Y} \left[\Omega + 2 \frac{m_2}{b} \omega \left(1 - \frac{M_1}{2R_1} \right)^2 \frac{\bar{X}}{b} + \frac{m_2}{b} \Omega \left(1 - \frac{M_1}{2R_1} \right)^2 \Psi^2 \frac{R_1^2}{b^2} P_2(\bar{X}/R_1) \right], \\
n_{(1),ICC}^2 &= -\frac{\Psi}{1 - \frac{M_1}{2R_1}} \left[\Omega \bar{X} + 2 \frac{m_2}{b} \omega \left(1 - \frac{M_1}{2R_1} \right)^2 \frac{\bar{X}^2 - \bar{Z}^2}{b} + \frac{m_2}{b} \Omega \left(1 - \frac{M_1}{2R_1} \right)^2 \Psi^2 \frac{R_1^2}{b^2} \bar{X} P_2(\bar{X}/R_1) \right], \\
n_{(1),ICC}^3 &= -2 \frac{m_2}{b} \omega \left(1 - \frac{M_1}{2R_1} \right) \Psi \frac{\bar{Y} \bar{Z}}{b}.
\end{aligned} \tag{71}$$

This means that the lapse and shift of the $\bar{T} = 0$ slice in the inner zone (\mathcal{C}_1) and in inner corotating coordinates are given by

$$\begin{aligned}
\alpha_{(1),ICC} &= -n_{(1),ICC}^0 = \frac{1 - \frac{M_1}{2R_1}}{\Psi} \left[1 - \frac{m_2}{b} \left(1 - \frac{M_1}{2R_1} \right)^2 \Psi^2 \frac{R_1^2}{b^2} P_2(\bar{X}/R_1) \right], \\
\beta_{(1),ICC}^i &= -\alpha_{(1),ICC} n_{(1),ICC}^i.
\end{aligned} \tag{72}$$

Observe that the lapse of Eq. (72) goes through zero at $R_1 = M/2$. Apart from a small perturbation it closely resembles the standard Schwarzschild lapse in isotropic

coordinates.

The expressions for the extrinsic curvature, lapse and shift given up to this point are in two different coordinate systems since they live in different submanifolds. The post-Newtonian quantities valid in the near zone (\mathcal{C}_3) are given in harmonic corotating coordinates, while the black hole perturbation theory results valid in the inner zones ($\mathcal{C}_{1,2}$) are given in isotropic corotating coordinates. We will now apply the coordinate transformation found in Sec. VI, namely Eq. 40, to transform the inner zone expressions to harmonic corotating coordinates, thus dropping the label ICC in favor of the superscript (1). The result for the inner extrinsic curvature of black hole 1 is given by

$$\begin{aligned}
K_{11}^{(1)} &\approx 2K_{01}^{(1),ICC} J_1^x J_1^t + 2K_{02}^{(1),ICC} J_1^y J_1^t + 2K_{03}^{(1),ICC} J_1^z J_1^t + K_{11}^{(1),ICC} J_1^{x2} + K_{22}^{(1),ICC} J_1^{y2} + K_{33}^{(1),ICC} J_1^{z2} \\
&\quad + K_{00}^{(1),ICC} J_1^{t2} + 2K_{12}^{(1),ICC} J_1^x J_1^y + 2K_{23}^{(1),ICC} J_1^y J_1^z + 2K_{13}^{(1),ICC} J_1^x J_1^z, \\
K_{22}^{(1)} &\approx K_{11}^{(1),ICC} J_2^{x2} + K_{22}^{(1),ICC} J_2^{y2} + K_{33}^{(1),ICC} J_2^{z2} + 2K_{12}^{(1),ICC} J_2^x J_2^y + 2K_{23}^{(1),ICC} J_2^y J_2^z + 2K_{13}^{(1),ICC} J_2^x J_2^z, \\
K_{33}^{(1)} &\approx K_{11}^{(1),ICC} J_3^{x2} + K_{22}^{(1),ICC} J_3^{y2} + K_{33}^{(1),ICC} J_3^{z2} + 2K_{12}^{(1),ICC} J_3^x J_3^y + 2K_{23}^{(1),ICC} J_3^y J_3^z + 2K_{13}^{(1),ICC} J_3^x J_3^z, \\
K_{12}^{(1)} &\approx K_{13}^{(1),ICC} (J_2^x J_1^z + J_1^x J_2^z) + K_{23}^{(1),ICC} (J_2^y J_1^z + J_1^y J_2^z) + K_{12}^{(1),ICC} (J_2^x J_1^y + J_1^x J_2^y) + K_{33}^{(1),ICC} J_1^z J_2^z + \\
&\quad K_{22}^{(1),ICC} J_1^y J_2^y + K_{11}^{(1),ICC} J_1^x J_2^x + K_{03}^{(1),ICC} J_1^t J_2^z + K_{02}^{(1),ICC} J_1^t J_2^y + K_{01}^{(1),ICC} J_1^t J_2^x, \\
K_{13}^{(1)} &\approx K_{13}^{(1),ICC} (J_3^x J_1^z + J_1^x J_3^z) + K_{23}^{(1),ICC} (J_3^y J_1^z + J_1^y J_3^z) + K_{12}^{(1),ICC} (J_3^x J_1^y + J_1^x J_3^y) + K_{33}^{(1),ICC} J_1^z J_3^z + \\
&\quad K_{22}^{(1),ICC} J_1^y J_3^y + K_{11}^{(1),ICC} J_1^x J_3^x + K_{03}^{(1),ICC} J_1^t J_3^z + K_{02}^{(1),ICC} J_1^t J_3^y + K_{01}^{(1),ICC} J_1^t J_3^x, \\
K_{23}^{(1)} &\approx K_{11}^{(1),ICC} J_2^x J_3^x + K_{22}^{(1),ICC} J_2^y J_3^y + K_{33}^{(1),ICC} J_2^z J_3^z + K_{12}^{(1),ICC} (J_2^x J_3^y + J_3^x J_2^y) + K_{23}^{(1),ICC} (J_2^y J_3^z + J_3^y J_2^z) \\
&\quad + K_{13}^{(1),ICC} (J_2^x J_3^z + J_3^x J_2^z),
\end{aligned} \tag{73}$$

where all components still have errors of $O(R_1/b)^3$. The extrinsic curvature in harmonic corotating coordinates in submanifold \mathcal{C}_2 can be obtained from the above equation by the symmetry transformation discussed in Eq. (41). In Fig. 11 we have plotted the xy component of the extrinsic curvature along the x axis. Observe that the behavior of the post-Newtonian solution (dashed line) is different

from that of the black hole perturbation solution close to the black hole, where the latter diverges more abruptly.

Similarly, the lapse and shift in harmonic corotating coordinates corresponding to the inner zone of black hole

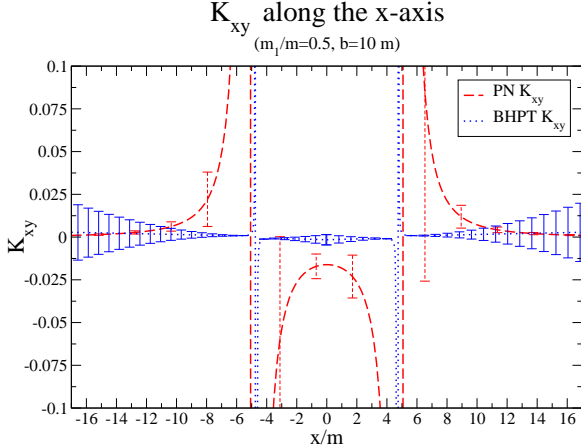


FIG. 11: This figure shows the xy component of the near zone (dashed line) extrinsic curvature, as well as the inner zone curvature obtained via black hole perturbation theory. This plots assume the test case, with equal mass black holes and $m/b = 1/10$.

1 are given by

$$\begin{aligned} \alpha_{(1)} &= \frac{1}{n_0^{(1)}} = -n_0^{(1)} = J_0^t \alpha_{(1),ICC}, \\ \beta_{(1)}^i &= -\alpha_1 n_1^i, \end{aligned} \quad (74)$$

where again the lapse and shift for the inner zone around black hole 2 (\mathcal{C}_2) can be obtained by the symmetry transformation mentioned above. In these equations, the normal vector is given by

$$n_{(1)}^\mu = J_\nu^\mu n_{(1),ICC}^\nu, \quad (75)$$

where the Jacobian matrix J_ν^μ has been defined in Eq. (43).

Note that $\alpha_{(1)}$ in Eq. (74) has the same zeros as $\alpha_{(1),ICC}$ and, thus, $\alpha_{(1)}$ also changes sign at $R_1 = M/2$. Furthermore, since $J_0^0 = 1 + O(m/b)$ the inner zone lapse $\alpha_{(1)}$ equals $\alpha_{(1),ICC}$ up to a perturbation of order $O(m/b)$ and thus $\alpha_{(1)}$ is equal to the standard lapse of Schwarzschild in isotropic coordinates plus a perturbation of order $O(m/b)$. These features are borne out by the plot in Fig. 12 which shows the global lapse along the x-axis.

Due to the piecewise nature of these solutions, there will be discontinuities on a 2-sphere located at some matching radius inside of the buffer zone. In order to eliminate these discontinuities, we use the same transition functions used for the metric in Eq. (49) with the same parameters. In this manner, we obtain a global extrinsic curvature, lapse and shift given by

$$\begin{aligned} K_{ij}^{(global)} &= G(x) \left\{ F_1(R_1) K_{ij}^{(1)} + [1 - F_1(R_1)] K_{ij}^{(3)} \right\} + [1 - G(x)] \left\{ F_2(R_2) K_{ij}^{(2)} + [1 - F_2(R_2)] K_{ij}^{(3)} \right\}, \\ \alpha_{(global)} &= G(x) \left\{ F_1(R_1) \alpha_{(1)} + [1 - F_1(R_1)] \alpha_{(3)} \right\} + [1 - G(x)] \left\{ F_2(R_2) \alpha_{(2)} + [1 - F_2(R_2)] \alpha_{(3)} \right\}, \\ \beta_{(global)}^i &= G(x) \left\{ F_1(R_1) \beta_{(1)}^i + [1 - F_1(R_1)] \beta_{(3)}^i \right\} + [1 - G(x)] \left\{ F_2(R_2) \beta_{(2)}^i + [1 - F_2(R_2)] \beta_{(3)}^i \right\}. \end{aligned} \quad (76)$$

Fig. 13, 14 and 15 show the global lapse, shift and extrinsic curvature with the transition functions. In these graphs, the error bars have been set at $E_{KBHPT} = 6(m/b)(r/b)^3(v/r)$ and $E_{KPN} = 4(m/r)^2(v/r)$, where the factors of 6 and 4 come from taking derivatives of the previous error estimates. Observe that the absolute error in the extrinsic curvature is $O(m/b)^{1/2}$ smaller than that of the metric. This is a reflection of the fact that the first non-trivial term in the extrinsic curvature appears at $O(m/b)^{3/2}$, as mentioned earlier.

As already mentioned, the initial data constructed by the methods above leads to an error in the constraints of the full theory, about $O(2, 4)$ in the Hamiltonian constraint. This error can be sufficiently small compared to other sources of numerical error such that solving the constraints more accurately is not required. In any case, one could use this solution as input to York's conformal method [6] and compute a numerical solution to the full

constraints. Somewhat surprisingly, standard PN data (without matching) has not yet been used for the generation of numerical black hole initial data except in Ref. [10], which is based on the PN data of Ref. [30]. We leave it to future work to explore similar techniques for the data set presented here.

The 3-metric $g_{ij}^{(global)}$ and extrinsic curvature $K_{ij}^{(global)}$ given in Eqs. (55) and (76) can now be used as initial data for black hole binaries. Recall however, that the data only approximately satisfy the constraints of general relativity to order $O(m/b)^6$ in the inner zone and $O(m/r)^2$ in the near zone. In order to obtain initial data that satisfy the constraints exactly, it will be necessary to project the data given in this paper to the constraint hypersurface. However, since this data is already significantly close to this surface, sensible projection methods should *not* alter much the astrophysical content of the initial data.

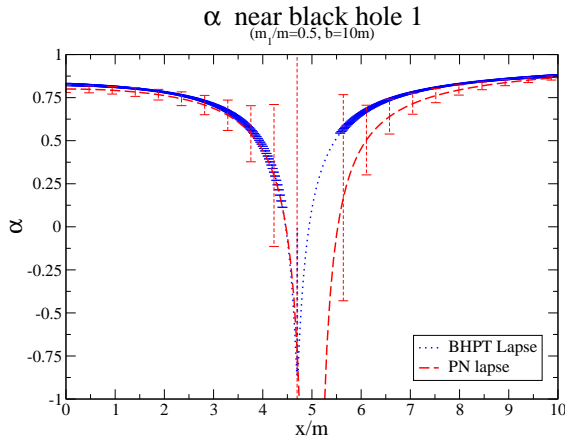


FIG. 12: This figure shows the near zone (dashed line) and the inner zone lapse (solid line) along the x-axis. Observe that the lapse crosses zero at the event horizon, whereas the near zone lapse is already negative there.

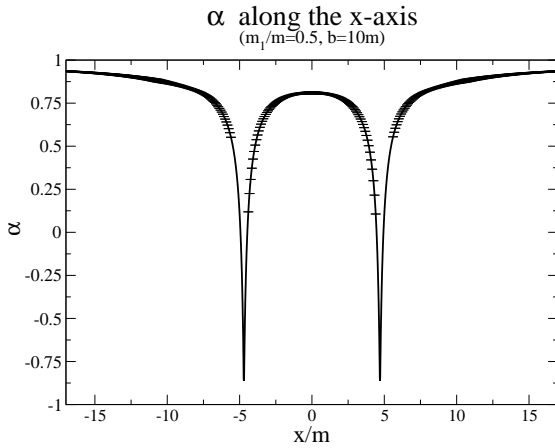


FIG. 13: This figure shows the global lapse along the x-axis with the transition function.

If this data is to be evolved, it is necessary to choose a lapse and a shift. The choice presented in this section is natural in the sense that it is close to quasi-equilibrium. In other words, with the lapse and shift presented in this section, the 3-metric and extrinsic curvature should evolve slowly. However, since our lapse is not everywhere positive, some evolution codes may have trouble evolving the initial data with the lapse presented here. If this is the case we can simply replace the above lapse with a positive function at the cost of losing manifest quasi-equilibrium, but without changing the physical content of the initial data or the results of the evolution.

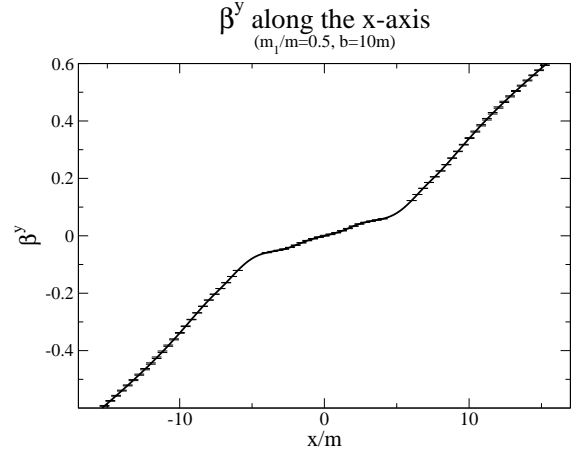


FIG. 14: This figure shows the global shift vector along the x-axis with the transition function.

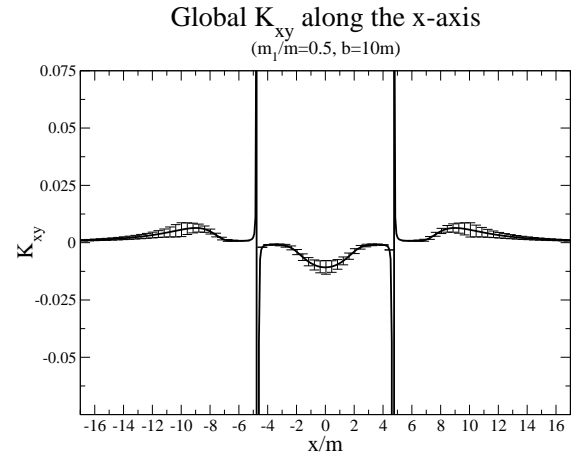


FIG. 15: This figure shows the global xy component of the extrinsic curvature along the x-axis with the transition function.

IX. CONCLUSIONS

We have constructed initial data for binary black hole systems (whose component masses need not be comparable) by calculating a uniform global approximation to the spacetime via asymptotic matching of locally good approximations. The manifold was first divided into three submanifolds: two inner zones (one for each hole), \mathcal{C}_1 and \mathcal{C}_2 ($r_A \ll b$) equipped with isotropic coordinates; and one near zone, \mathcal{C}_3 ($r_A \gg m_A$ and $r \ll \lambda/2\pi$), equipped with harmonic coordinates. In the near zone, the metric was approximated with a post-Newtonian expansion, while in each inner zone the metric was approximated with a perturbative tidal expansion of Schwarzschild geometry. Each approximate solution depends on small parameters locally defined on each submanifold. We have shown that these submanifolds overlap in two buffer zones, \mathcal{O}_{13} and

\mathcal{O}_{23} (4-volumes), given by the intersection of the inner zones with the near zone, *i.e.* $m_A \ll r_A \ll b$. Inside each buffer zone, two different approximations for the metric were simultaneously valid and hence we were allowed to asymptotically match them inside this 4-volume.

The matching procedure consisted of first expanding both approximate metrics asymptotically inside of the buffer zone. After transforming to the same gauge, these asymptotic expansions were then set asymptotic to each other, leading to a set of partial differential equations. After solving these differential systems, asymptotic matching returned a coordinate transformation, ϕ_{13} and ϕ_{23} , between submanifolds and matching conditions ψ_{13} and ψ_{23} , that relate parameters native to different charts. A piecewise global metric was then obtained by transforming all metrics to harmonic coordinates with the set $\{\phi_{nm}; \psi_{nm}\}$.

Once a piecewise global metric was found, the spatial metric and extrinsic curvature were calculated in each zone by choosing a spatial hypersurface, with the standard 3 + 1 decomposition. This initial data was then transformed in the same manner as the 4 metric. Due to the inherent piecewise nature of this data, we found discontinuities of order $O(3/2, 3)$ or smaller inside the buffer zone. We constructed transition functions to remove the remaining small discontinuities in metric components and spikes in derivatives. With these functions, we constructed a global uniform approximation to the metric valid everywhere in the manifold with errors $O(m/b)^6$ near the black holes and $O(m/r)^2$ far away from either of them.

This uniform global approximation of the metric can be extended within $b = 10m$ but not inside $b \approx 7m$. This criterion approximately corresponds to the inner zones of the two black holes coming into contact with no intervening post-Newtonian near zone in which to match. However, since there is no precise knowledge of the region of convergence of the PN series, it is unknown precisely where the near zone vanishes.

We also constructed a natural lapse, shift, and extrin-

sic curvature, all of which are needed for numerical evolutions. The lapse was found to possess the expected feature that it becomes negative inside the horizon of either black hole. Some numerical codes might find this feature undesirable, in which case the lapse can be replaced by some positive function at the cost of losing approximate quasi-stationarity.

In conclusion, we have constructed astrophysically realistic initial data for a binary black hole system that satisfies the constraints to order $O(2, 4)$ in the inner zone, and to order $O(m/r)^2$ in the near zone. Nevertheless, we should note that this data is not yet completely realistic, since it makes use of perturbative expansions of low order (*e.g.*, the near zone metric is built from a 1 PN expansion). However, the data presented in this paper does possess the first astrophysically realistic deviations from conformal flatness due to the tidal perturbations of the metric in the inner zone. Moreover, this paper introduces a method that could be repeated to higher order at the cost of more algebra. Particularly interesting would be the inclusion of $O(m/b)^{5/2}$ terms in the post-Newtonian metric arising from gravitational waves and terms of $O(r/b)^3$ which were recently computed [21]. Our method might also be extended to spinning black holes, which are more physically realistic.

Acknowledgments

We thank Thomas Baumgarte, Carl Bender, Lee Lindblom, Eric Poisson, Kip Thorne, Qinghai Wang, and Clifford Will for useful discussions and insightful comments.

We acknowledge the support of the Institute for Gravitational Physics and Geometry and the Center for Gravitational Wave Physics, funded by the National Science Foundation under Cooperative Agreement PHY-01-14375. This work was also supported by NSF grants PHY-02-18750, PHY-02-44788, and PHY-02-45649.

[1] T. W. Baumgarte and S. L. Shapiro, Phys. Rept. **376**, 41 (2003), and references therein, gr-qc/0211028.
[2] G. B. Cook, Phys. Rev. D **50**, 5025 (1994).
[3] R. A. Matzner, M. F. Huq, and D. Shoemaker, Phys. Rev. D **59**, 024015 (1999).
[4] T. W. Baumgarte, Phys. Rev. D **62**, 024018 (2000), gr-qc/0004050.
[5] P. Marronetti and R. A. Matzner, Phys. Rev. Lett. **85**, 5500 (2000), gr-qc/0009044.
[6] G. B. Cook, Living Rev. Rel. **3**, 5 (2000), and references therein, gr-qc/0007085.
[7] P. Grandclément, E. Gourgoulhon, and S. Bonazzola, Phys. Rev. D **65**, 044021 (2002), gr-qc/0106016.
[8] H. P. Pfeiffer, G. B. Cook, and S. A. Teukolsky, Phys. Rev. D **66**, 024047 (2002), gr-qc/0203085.
[9] B. D. Baker (2002), gr-qc/0205082.
[10] W. Tichy, B. Brügmann, M. Campanelli, and P. Diener, Phys. Rev. D **67**, 064008 (2003), gr-qc/0207011.
[11] W. Tichy, B. Brügmann, and P. Laguna, Phys. Rev. D **68**, 064008 (2003), gr-qc/0306020.
[12] W. Tichy and B. Brügmann, Phys. Rev. D **69**, 024006 (2004), gr-qc/0307027.
[13] H.-J. Yo, J. N. Cook, S. L. Shapiro, and T. W. Baumgarte, Phys. Rev. D **70**, 084033 (2004), gr-qc/0406020.
[14] G. B. Cook and H. P. Pfeiffer (2004), gr-qc/0407078.
[15] L. Blanchet, Living Rev. Rel. **5**, 3 (2002), and references therein, gr-qc/0202016.
[16] K. S. Thorne and J. B. Hartle, Phys. Rev. D **31**, 1815 (1984).
[17] C. M. Bender and S. A. Orszag, *Advanced mathematical methods for scientists and engineers 1, Asymptotic methods and perturbation theory* (Springer, New York, 1999).

- [18] K. Alvi, Phys. Rev. **D61**, 124013 (2000), gr-qc/9912113.
- [19] N. Jansen and B. Brügmann (2002), unpublished.
- [20] L. Blanchet, T. Damour, G. Esposito-Farese, and B. R. Iyer, Phys. Rev. Lett. **93**, 091101 (2004), gr-qc/0406012.
- [21] E. Poisson (2005), gr-qc/0501032.
- [22] W. L. Burke and K. S. Thorne, in *Relativity*, edited by M. Carmeli, S. I. Fickler, and L. Witten (Plenum Press, 1970), pp. 209–228.
- [23] W. L. Burke, J. Math. Phys. **12**, 401 (1971).
- [24] P. D. D'Eath, Phys. Rev. **D12**, 2183 (1975).
- [25] P. D. D'Eath, Phys. Rev. **D11**, 1387 (1975).
- [26] C. M. Will and A. G. Wiseman, Phys. Rev. **D54**, 4813 (1996), gr-qc/9608012.
- [27] L. Blanchet, G. Faye, and B. Ponsot, Phys. Rev. **D58**, 124002 (1998), gr-qc/9804079.
- [28] M. Visser and N. Yunes, Int. J. Mod. Phys. **A18**, 3433 (2003), gr-qc/0211001.
- [29] K. Alvi, Phys. Rev. **D67**, 104006 (2003), gr-qc/0302061.
- [30] P. Jaranowski and G. Schafer, Phys. Rev. **D57**, 7274 (1998), gr-qc/9712075.